J. Fluid Mech. (1997), *vol.* 351, *pp.* 253–288. Printed in the United Kingdom

The effects of successive distortions on a turbulent boundary layer in a supersonic flow

By DOUGLAS R. SMITH† AND ALEXANDER J. SMITS

Gas Dynamics Laboratory, Princeton University, Princeton, NJ 08544-0710, USA

(Received 18 July 1996 and in revised form 6 May 1997)

Experiments were conducted to investigate the response of a high-Reynolds-number turbulent boundary layer in a supersonic flow to the perturbation presented by a forward-facing ramp. Two ramps were used: one with sharp corners, the other with rounded corners having radii of curvature equal to 15 initial boundary layer thicknesses. The flow was turned through 20° in each of the compressions and expansions. Hence, there was no net change in the flow direction over the ramps and only a small change in free-stream conditions due to the entropy increase across relatively weak shocks. The two experiments gave similar results. In the middle of the relaxing boundary layer, the streamwise Reynolds stress undershot the undisturbed levels and exhibited a response similar to that observed in subsonic boundary layer flows recovering from an impulse of streamline curvature (Smits, Young & Bradshaw 1979*b*). The turbulent shear stress vanished throughout most of the boundary layer, and an overall destruction of the turbulence production mechanisms was apparent as the boundary layer exhibited a slow recovery.

1. Introduction

Here, we discuss two experiments designed to study the effects of successive distortions on a high-Reynolds-number turbulent boundary layer in supersonic flow with a free-stream Mach number of 2.89. In the first experiment (Ramp A), the flow passed over a 20° compression corner followed by a 20° expansion corner with a distance between the corners of about $6\delta_\circ$, where $\delta_\circ$ was the incoming boundary layer thickness. In the second experiment (Ramp B), the compression and expansion corners were replaced by curved compression and expansion surfaces with radii of curvature equal to $15\delta_\circ$, but retained the turning angles and the step height as on Ramp A (see figure 1).

As the flow passed over these ramps, the boundary layer was subjected first to an adverse pressure gradient combined with concave streamline curvature and bulk compression, and second to a favourable pressure gradient combined with convex streamline curvature and bulk dilatation. On Ramp A, the initial turning at the compression corner resulted in a shock wave/boundary layer interaction. The subsequent expansion occurred through a centred expansion fan. On Ramp B, the concave and convex streamline curvatures were distributed over longer streamwise distances than on Ramp A, and therefore the pressure gradients were less severe. In

† Current address: The Boeing Company, Mailcode S1067126, PO Box 516, St Louis, MO 63166, USA.

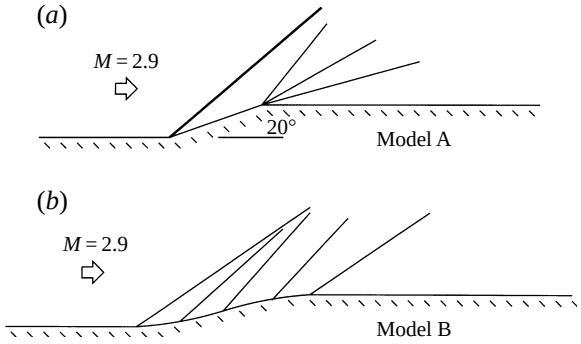

FIGURE 1. Schematics of the flow geometries: (*a*) Ramp A; (*b*) Ramp B.

particular, the shock associated with the concave curvature was not formed until well outside the boundary layer, and within the boundary layer the compression occurred through a compression fan rather than a shock wave/boundary layer interaction. On Ramps A and B, however, there was no net change in flow direction over the ramp; therefore, the upstream and the downstream free-stream conditions were effectively the same except for a small shock loss on Ramp A.

These experiments, on the response to successive regions of compression and expansion, represent a logical extension of previous work in this area, as the effects of isolated compressions and expansions have been studied extensively in the past. For example, the behaviour of turbulent boundary layer/shock wave interactions generated by compression corners has been investigated over a wide range of Mach numbers and turning angles (Settles, Fitzpatrick & Bogdonoff 1979; Debiève, Gouin & Gaviglio 1982; Dolling & Murphy 1983; Ardonceau 1984; Smits & Muck 1987), and there have been a number of studies of the effect of centred expansions (Dussauge & Gaviglio 1987; Smith & Smits 1991; Arnette, Samimy & Elliot 1993). Such flows are now reasonably well understood, at least in a qualitative sense, so that we can broadly anticipate the response of the boundary layer.

1.1. *Compression- and expansion-corner flows*

In compression-corner flows, the boundary layer experiences the combined effects of an adverse pressure gradient, concave streamline curvature, bulk compression, shock unsteadiness, and if the pressure rise is strong enough, flow separation. The wall stress typically decreases sharply near the start of the interaction, but quickly recovers as the boundary layer thins in response to the overall compression, overshooting the upstream level before eventually recovering to a level appropriate to the new Reynolds number and Mach number on the ramp. At the same time, the turbulence levels increase dramatically through the interaction and appear to relax only slowly. The shear stress is generally affected less than the normal stresses, and structure parameters, such as $a_1 \equiv -\overline{u'v'}/q^2$, are strongly distorted. With the boundary layer responding to the combined effects of many distortions, it is difficult to conclude from the available data the specific contributions of, say, concave streamline curvature and bulk compression to the distortion, although Selig & Smits (1991) showed that shock unsteadiness does not contribute significantly to the turbulence amplification, in contrast to the earlier speculations of Smits & Muck (1987). The data also show that when the flow is compressed on a curved wall with a short radius of curvature, the boundary layer turbulence is amplified to a significantly larger degree than when the

compression occurs on a curved wall with a larger radius of curvature, or when the compression is due to a wave system incident on a flat wall (Spina, Smits & Robinson 1994).

For expansion-corner flows, the response is almost the exact inverse to that seen in compression-corner flows. The boundary layer experiences the combined effects of a favourable pressure gradient, convex streamline curvature and bulk dilatation. In response to the expansion, the boundary layer thickness increases, and the wall stress rapidly decreases before beginning a relaxation where its value appears to approach asymptotically its undisturbed value at the new Reynolds number. The streamwise Reynolds stress falls sharply and recovers slowly. The response of the other turbulent stresses is unknown since they have not been measured in these flows. However, Dussauge & Gaviglio (1987) and Smith & Smits (1991) have demonstrated that a calculation using the Reynolds stress equations closed with rapid distortion approximations (RDA) can give good predictions of the measured turbulence behaviour in the initial boundary layer response where such RDA calculations are valid. Smith & Smits have also suggested that these methods may be used to calculate the response of the full Reynolds stress tensor. Furthermore, these calculations have indicated that the bulk dilatation is the most important influence on the Reynolds stress evolution; the effect of convex curvature was found to be small, at least in the initial boundary layer response where this calculation is valid.

1.2. *Curved wall flows*

Flows where the perturbations are not produced by compression or expansion corners, but where they are produced by curved walls, as on Ramp B, have also been studied extensively. In particular, supersonic flows over concavely curved walls have been investigated over a wide range of turning angles and radii of curvature (Sturek & Danberg 1972*a,b*; Laderman 1980; Jayaram, Taylor & Smits 1987; Donovan, Spina & Smits 1994). A typical feature of these flows with concave streamline curvature is the appearance of a 'dip' in the velocity profile below the log-law before rising above it in the wake region. The turbulence data from these studies were recently analysed by Spina *et al.* (1994), who noted that at Mach 2.9 the amplification of the longitudinal Reynolds stress, for a given pressure rise (that is, for a given turning angle), was smaller when the strength of the pressure gradient was reduced. In contrast, the amplification of the Reynolds shear stress appeared to depend on the overall pressure rise rather than the pressure gradient. For rapid distortions along curved walls where the turbulence time scales were long compared to the time of the distortion, Jayaram *et al.* (1989) found that RDA methods can give reasonable predictions of the initial amplification of the normal and shear stresses in the boundary layer for $y/\delta > 0.2$.

In subsonic turbulent boundary layers, concave curvature in the streamwise direction introduces longitudinal vortices according to a mechanism similar to that responsible for producing Taylor–Görtler vortices in laminar flows (Tani 1962). These longitudinal roll cells tend to be spaced in the spanwise direction with a reasonably regular spacing of one to two boundary layer thicknesses, and once established they are very stable in location and strength. Although they are generally weak, in that their tangential velocity is at least an order-of-magnitude smaller than the free-stream velocity, they can have strong effects on the turbulence. For example, Smits, Young & Bradshaw (1979*b*) found that downstream of an impulse in concave curvature the shear stress differed by up to a factor of two in the spanwise direction. The low level was found in the region where the secondary flow was towards the wall (that is, a 'crest' in the spanwise C_f distribution), and the high level was found where the flow

was away from the wall (a 'trough' in the C_f distribution). The corresponding C_f values differed by about 20% from the crest to the trough.

In some particular flows with concave curvature, Taylor–Görtler vortices have not been observed. In the study by Smits, Eaton & Bradshaw (1979*a*), where the flow developed on a cylindrical forebody before diverging on a cone, the boundary layer experienced the combined effects of concave curvature and divergence. Here, steady vortices were not detected. However, it is possible that unsteady vortices were formed, without a preferred spanwise position, or that the vortices originated intermittently at different spatial locations. The measurements were not designed to detect such unsteady motions, so it is only possible to speculate. It is also possible that the roll cells did not form at all because of a nonlinear interaction between concave curvature (which amplifies longitudinal vorticity) and divergence (which amplifies spanwise vorticity).

In separated supersonic flows, surface oil flow visualizations in the region of reattachment suggest that steady Taylor–Görtler vortices can also occur in compressible flows (Roshko & Thomke 1966). Visualizations of the separation and reattachment lines in compression-corner flows similarly suggest the existence of longitudinal vortices, with a spanwise spacing similar to that seen in incompressible flows. Selig *et al.* (1989) suggested that longitudinal vortices could be the cause of a bimodal p.d.f. in the mass-flux fluctuations downstream of a 24° compression corner, since they are an effective mechanism for sweeping low-momentum fluid up from the near-wall regions. However, no evidence of steady Taylor–Görtler-like vortices was found in any of the attached flows on curved walls studied by Jayaram *et al.* (1987) and Donovan *et al.* (1994). It is again possible that nonlinear effects may have prevented their appearance. For example, it was suggested by Green (see Bradshaw 1973; Smits *et al.* 1979*a*) that bulk compression acts in many respects similarly to lateral divergence. If it is true that Taylor–Görtler vortices do not form in subsonic boundary layer flows when concave curvature and divergence act together, then by extension it may not be surprising that when concave curvature and dilatation occur together, Taylor–Görtler vortices again appear to be absent.

A criterion for the onset of steady Taylor–Görtler vortices in compressible flows with concave curvature was developed by Smits & Dussauge (1996), as follows. According to Schlichting (1979), Taylor–Görtler vortices first appear in a laminar, incompressible boundary layer on a concavely curved wall when the characteristic parameter, the Görtler number G_T,

$$G_T = \frac{U_e\theta}{\nu}\left(\frac{\theta}{R}\right)^{1/2},$$

exceeds a certain value. Stability calculations give the neutral curve as a function of a non-dimensional wavelength. Tani (1962) suggested that this criterion could be applied to turbulent flows by using the same characteristic length scale, θ, and simply replacing the molecular viscosity by the eddy viscosity. If it is assumed that the eddy viscosity in the outer layer is given by

$$\nu_t = 0.018U_e\delta^* \tag{1.1}$$

(Clauser 1956) then

$$G_T = \frac{\theta}{0.018\delta^*}\left(\frac{\theta}{R}\right)^{1/2}, \tag{1.2}$$

which indicates that the appearance of longitudinal vortices in a turbulent flow is

a weak function of Reynolds number since the shape factor varies somewhat with Reynolds number. Bradshaw (1973) pointed out that the direct use of the neutral curve for the Blasius profile is not realistic, but Tani's measurements agreed reasonably well with this simple proposal. Note that the Görtler number for turbulent flow can also be written as

$$G_T = \frac{(\theta/\delta)^{1.5}}{0.018\,(\delta^*/\delta)} \left(\frac{\delta}{R}\right)^{1/2}. \tag{1.3}$$

The analysis can be extended to compressible flow by assuming that the length scale remains unchanged and that the eddy viscosity is still given by (1.1). In other words, the Görtler number for a compressible turbulent flow is given by (1.3), where it is recognized that the momentum and displacement thicknesses are a strong function of Mach number. Some typical values may then be found for the lower limit on δ/R where longitudinal vortices are expected to appear, corresponding to the neutral curve calculated by Smith (1955) and a fixed wavelength of 2δ (the weak dependence of the Görtler number on Reynolds number was ignored). As the free-stream Mach number increases from 0, to 1, to 3, to 5, $(\delta/R)_s$ increases from 0.003, to 0.005, to 0.03, to 0.11, respectively. That is, the analysis predicts a strong increase in stability with increasing Mach number. Most of the Mach 3 curved-wall cases, see Jayaram *et al.* (1987) and Donovan *et al.* (1994), exceed this rather crude criterion, but not by very much (the maximum value of δ/R was 0.1), and it seems likely that the absence of Taylor–Görtler vortices in these attached flows is at least partly due to the stabilizing influence of Mach number. For the separated flows, the distortion of the mean velocity profile will influence the stability calculation, and the appearance of an inflection point will obviously make the layer more unstable in every sense.

In contrast to the case with concave curvature, flows with convex curvature have received relatively little attention, but recently Johnson (1993) presented measurements in a Mach 2.45 flow where the non-dimensional radius of curvature of the expansion corner $\delta_\circ/R$ was varied from 0.067 to 0.2, to 1, to ∞ while the overall turning angle was maintained at 15°. The incoming flow was still recovering from the distortion presented by a 10° concavely curved wall placed $3\delta_\circ$ upstream; however, the incoming flow was the same for each case, and the effect of varying the convex radius of curvature can still be inferred. The downstream velocity profiles all displayed a 'negative dip', in that the velocity distribution rose above the log-law in the near-wall region (in contrast to the experiments with concave curvature where the velocity distribution fell below the log-law in the near-wall region). Johnson found a strong suppression of the turbulence levels downstream of the expansion, but the suppression and subsequent relaxation of the longitudinal velocity fluctuations was remarkably similar in all four cases suggesting that the overall pressure drop (or, equivalently, the total turning angle) was the dominant influence rather than the strength of the pressure gradient.

1.3. *Impulsive disturbances*

In the experiments discussed so far, results were obtained on the initial response of the boundary layer to 'impulsive' disturbances where two step changes of opposite character occur successively. A step change is taken to mean, for example, the change experienced by an undisturbed boundary layer in contact with a wall which suddenly changes from being flat to being curved. If the wall then becomes flat again a short distance downstream (the second, opposite, step change), the boundary layer is said to experience an impulse in curvature (Smits & Wood 1985). The relaxation behaviour is also of great interest. In particular, Smits *et al.* (1979*b*) found that the downstream

relaxation of subsonic boundary layers to impulses in convex and concave curvature was surprising in some respects. In the initial response, the effects of streamline curvature were as expected with the destabilizing effects of concave curvature causing an increase in the Reynolds stresses and the stabilizing effects of convex curvature causing a decrease. Further downstream, however, the stress profiles did not return monotonically to their 'equilibrium' levels but instead displayed a kind of second-order response where the stress levels eventually undershot the equilibrium levels. In this case, the net effect of an impulse in destabilizing curvature was a boundary layer with very low levels of all turbulent stresses. Similarly, downstream of the convex curvature, the stress levels overshot the equilibrium levels, and the net effect of an impulse in stabilizing curvature was a boundary layer with very high levels of all turbulent stresses. Analogous observations were made in subsequent studies by Gillis & Johnston (1983) and Alving, Smits & Watmuff (1990). The eventual relaxation to some equilibrium state, if it exists, is in all cases extremely slow, typically of order $100\delta_\circ$.

In the experiments described here, boundary layers in supersonic flow experience double impulses, that is, four successive step changes in wall curvature (from flat to concave, concave to flat, flat to convex and convex to flat). The final flow direction is parallel to the upstream flow, so that no net change in flow direction occurs through the distortion. The flow then proceeds downstream on the flat wall where the relaxation behavior can be studied.

Recently Bandyopadhyay & Ahmed (1993) studied the response of a subsonic boundary layer to similar successive perturbations. They found that the relaxing boundary layer had a sustained lower skin friction than an equilibrium boundary layer (wall A) at the same Reynolds number, and the recovery was not complete at the final measurement station 100 initial momentum thicknesses downstream of the end of curvature. The longitudinal Reynolds stress in the outer layer first displayed levels lower than in the incoming boundary layer but the levels near the wall were much higher. Further downstream, these elevated stress levels move out from the wall in what Smits *et al.* (1979*b*) called a 'stress bore' so that the downstream profiles demonstrate high levels of stress throughout the boundary layer.

The first detailed experiments in supersonic boundary layer flows with successive distortions were made by Zheltovodov *et al.* (1990). In that study, a flow with an initial Mach number of 2.9 passed over a 25° compression corner followed by a 25° expansion corner. The configuration was very similar to that used in the experiment here for Ramp A. However, only the streamwise component of the Reynolds stress was measured. This component showed a strong decrease in the recovery region, and the stress levels fell below the undisturbed levels in the outer part of the layer. Unfortunately, these hot-wire results are difficult to interpret accurately, as the boundary layers were quite thin, and the turbulence levels were considerably underestimated because of poor spatial resolution, particularly in the upstream, undisturbed boundary layer. As the boundary layer thickness increased further downstream the resolution of the probes improved. However, in comparing the upstream and downstream turbulence levels, a part of the observed increase in the relaxation region was due to the improved resolution of the measurements and so any estimates of turbulence amplification are inaccurate.

The study by Johnson (1993) of the flow passing over concave compression surfaces followed by convex expansion surfaces at a free-stream Mach number of 2.45 was mentioned earlier. In that study, the primary interest was in the relaminarization of the downstream flow by the stabilizing influence of bulk dilatation, but Johnson showed

that for two different upstream disturbances (a concave ramp with $\delta_\circ/R = 0.033$ with a total turning angle of 10°, and a compression ramp with turning angle of 15°) the turbulence levels immediately downstream of a 15° expansion were essentially the same and considerably lower than in an undisturbed boundary layer at the same Reynolds and Mach numbers. Further downstream, the levels remained low and at the last station, located $10\delta_\circ$ downstream of the expansion, still showed no tendency to recover.

In the experiments presented here, we are interested in the relaxation behaviour of turbulence, in contrast to the studies by Zheltovodov *et al.* (1990) and Johnson (1993). We aim to determine the principal physical mechanisms which govern the recovery process in the boundary layer downstream of the ramp. Our primary interest is the interaction of compression distortions with expansion distortions, unlike Johnson who focused on the effects of bulk dilatation and relaminarization, and used a compression ramp upstream of his expansion corner only because of the physical limitations imposed by his wind tunnel facility. Also, the advantage of the present study over Zheltovodov *et al.* (1990) was our ability to make two-component turbulence measurements, and to make more accurate and detailed turbulence measurements because our initial boundary layer thickness was relatively large (approximately 26 mm). These measurements included the response of the mean flow to the distortion and the initial response of the turbulent stresses and their subsequent relaxation. These results were compared with previous boundary layer measurements from single-step and impulsive perturbations performed in the same wind tunnel at the same Mach and Reynolds numbers. Through these comparisons, the interaction of successive impulses is analysed, and an attempt is made to identify the different influences of pressure gradient, compression/dilatation and curvature. In this respect, the RDA methods discussed earlier proved to be very useful.

In §2, the experimental facilities/layout and measurement methods will be briefly presented. The measurements made on the corner ramp (Ramp A) and on the curved ramp (Ramp B) are discussed in §3. Section 4 compares the boundary layer behaviour on the two ramps, and §5 considers the general reaction and relaxation behaviour of the turbulence in the boundary layer. Finally, §6 is reserved for conclusions and recommendations for future study.

2. Experimental details

All experiments were conducted in the high-Reynolds-number, supersonic wind tunnel located at Princeton University's Gas Dynamics Laboratory. The wind tunnel is a blowdown facility with a nominal free-stream Mach number of 3. For all tests, the stagnation chamber pressure was held constant at 689 kPa $\pm 0.7\%$. The stagnation temperature followed daily and seasonal variations, and also changed over the course of a run, decreasing at about 0.12 K s^{-1}. The boundary layer studied in the experiments developed on the floor of the wind tunnel, which was approximately adiabatic. Transition occurred naturally in the nozzle section, and downstream of the nozzle the boundary layer developed on the wall of the test section in a nominally zero pressure gradient. The characteristics of this boundary layer have been extensively documented (see Settles 1975; Spina & Smits 1987; Smits & Muck 1987), and the data demonstrate that the boundary layer is fully developed and self-preserving. The turbulence structure (inferred from ensemble-averaged statistics and cross-correlations of hot-wire signals) was documented in Spina & Smits (1987) and Spina, Donovan & Smits (1991). The spanwise variations in the mean flow properties of the incoming

Ma_{ref}	2.89
Re m^{-1}	6.3×10^7 m^{-1}
$P_\circ$	6.9×10^5 N m^{-2}
$T_\circ$	270 K
$T_w/T_\circ$	1.04
U_{ref}	580 m s^{-1}
ρ_{ref}	0.78 kg m^{-3}
P_w	2.2×10^4 N m^{-2}
$\delta_\circ$	23 mm
δ^*_{ref}	6.2 mm
θ_{ref}	1.1 mm
$(\overline{\rho U})_{ref}$	450 kg m^{-2} s

TABLE 1. Incoming flow conditions

boundary layer were extensively investigated by Jayaram *et al.* (1987). The spanwise wall-pressure and skin-friction distributions over a distance of ± 50 mm varied by less than $\pm 0.5\%$ and $\pm 4\%$, respectively, and no pattern was found in the variations which may indicate the presence of steady Taylor–Görtler vortices originating in the nozzle. The upstream boundary layer measurements made in this study agree closely with these earlier results. The free-stream flow conditions are summarized in table 1.

Two experiments were performed. In the first experiment, the flow passed over a forward facing step consisting of a 20° compression corner followed by a 20° expansion corner (Ramp A, figure 1*a*). Between the first and second corners, there was a flat wall 149 mm in length. Downstream of the second corner, there was a second region of flat wall, parallel to the upstream floor, which extended for 330 mm ($\approx 13\delta_\circ$). In the second experiment, the flow was also successively turned through the same 20° of compression and 20° of expansion, but the sharp corners of Ramp A were replaced by curved walls with radii of curvature equal to 350 mm ($\delta_\circ/R \approx 0.08$; Ramp B, figure 1*b*). For a compression surface under these flow conditions (that is in the same wind tunnel at the same Mach and Reynolds number), Donovan *et al.* (1994) found that the shock-wave forms outside of the boundary layer, and in this respect, the flow over Ramp B experienced a near-isentropic compression followed by an isentropic expansion. In both experiments, the interaction began at the same position relative to the wind tunnel nozzle, and the height of the ramps was the same, 50.8 mm. Table 2 lists the streamwise variations in the free-stream flow conditions for Ramps A and B.

In both experiments, the ramps did not span the wind tunnel. As the wind tunnel nozzle was two-dimensional, the tunnel sidewall boundary layers had pronounced three-dimensionality, and the interaction of the ramp flows with the sidewall boundary layers would have complicated the current study by making the mean flow three-dimensional. Aerodynamic fences were used to isolate the ramp distortions from the sidewall boundary layers and to maintain the two-dimensionality of the boundary layer flow through the distortions by minimizing the convergence or divergence of streamlines.

In each experiment, measurements were made both on and off the tunnel centreline. The off-centre measurements, taken at positions of $z = \pm 25.4$ mm, were used to check that the mean flow remained two-dimensional. The two-dimensionality of the flow was also checked using spanwise surface pressure and skin friction measurements.

	x (mm)	ρ_δ/ρ_{ref}	U_δ/U_{ref}	$\rho_\delta U_\delta/\rho_{ref}U_{ref}$	$\rho_\delta U_\delta^2/\rho_{ref}U_{ref}^2$
(*a*)	−41	0.9820	1.001	0.9830	0.9840
	76	2.104	0.8768	1.844	1.617
	114	2.102	0.8631	1.814	1.566
	232	1.047	0.9793	1.025	1.004
	283	1.041	0.9786	1.018	0.9967
	334	0.9806	0.9843	0.9652	0.9500
	385	1.050	0.9679	1.016	0.9837
	436	1.083	0.9668	1.047	1.012
(*b*)	−15	0.9914	1.000	0.9914	0.9914
	330	1.176	0.9766	1.148	1.121
	381	1.053	0.9728	1.025	0.9969
	432	1.060	0.9886	1.047	1.036
	483	1.080	0.9837	1.063	1.046
	533	1.108	0.9847	1.091	1.074
	584	1.215	0.9640	1.172	1.129

TABLE 2. Variation in boundary layer edge conditions (*a*) along Ramp A, (*b*) along Ramp B

The spanwise variations in the wall friction downstream of the distortions were less than 10% of the centreline value, and the distribution was similar to that observed in the upstream boundary layer flow. Spanwise variations in wall pressure were less than 5% at all locations on the two ramps. Surface streamlines were visualized by applying a thin layer of a kerosene-lampblack mixture on the surface of the model. They remained parallel throughout the distortion and relaxation regions (see Smith 1993 for further details), giving further indication that steady longitudinal vortices were not present in the flow over the surface of the ramps and further downstream.

The wall friction values were determined from a Preston tube measurement and the Clauser chart method. To apply the Clauser chart method in compressible boundary layers, the measured velocity profiles were first transformed into the incompressible plane using the van Driest (1951) compressibility transformation. In this transformation, it is assumed that the length scale distributions in subsonic and supersonic boundary layers follow the same distribution. Then, the fluid property variation due to viscous heating may be taken into account by using Crocco's law (or the relationship suggested by Walz 1966) to relate the velocity and temperature. An equivalent incompressible velocity can then be defined which appears to obey the usual scaling laws such as the incompressible form of the log-law over a very wide range of Mach and Reynolds numbers (see, for example, Fernholz & Finley 1980). The transformation assumes that the boundary layer is self-preserving which may not be strictly the case in a distorted boundary layer flow, but is a good approximation near the wall where the turbulence time scales are short and the boundary layer adjusts quickly to perturbations such as shock-wave boundary layer interactions.

The Preston tube data were reduced using the method of Bradshaw & Unsworth (1974), as corrected by Allen (1977). This reduction technique was chosen over other methods, for example Hopkins & Keener (1966), because it is based upon correlations in wall variables while the other methods use correlations based upon properties at the edge of the boundary layer. In distorted supersonic flows, a reduction method based on wall variables is intuitively appealing, as the conditions at the wall may be different to those at the boundary layer edge because of gradients of pressure across the boundary layer.

From a survey of skin friction measurements in perturbed supersonic flows, Smith *et al.* (1992) found that when the velocity profile displayed a region of logarithmic variation in the transformed plane the Preston tube and Clauser chart values of τ_w agreed very well, within 10%, even in flows with strong adverse pressure gradients. Kim, Lee & Settles (1991) have shown that Preston tube results also agree well with direct measurements of the skin friction in strongly perturbed supersonic boundary layer flows using the oil-drop technique, and it appears that the Preston tube is an effective tool for finding the skin friction variations in perturbed supersonic flows. On Ramp B, the Preston measurements shown for the convexly curved wall are intended mainly to convey the trend in the wall friction, since in regions of strong favourable pressure gradient, the calibration of a Preston tube is not clearly defined.

Hot-wire measurements were made using a constant-temperature anemometer system. The anemometers were DISA 55M01 units using 55M12 symmetrical bridges, and the hot-wire probes were constructed in-house (see Smith 1993 for details).

The use of normal and crossed hot wires in supersonic flows has been treated extensively by Kovásznay (1950), Smits, Hayakawa & Muck (1983), and Donovan & Spina (1992). For a hot wire operating at a high overheat ratio, the output of the anemometer can be related to the instantaneous mass-flux by

$$E^2 = L + MG(\phi)(\rho u)^n \tag{2.1}$$

where L and M are constants for a given wire determined from the calibration and $G(\phi)$ is the angular sensitivity function of the wire which is also determined by calibration. For a normal hot wire, $G(\phi = 0) = 1$, and the instantaneous mass flux is found by inverting this relation at each point in the sample. For a crossed wire, ϕ and ρu may be found from a second-order perturbation analysis of the hot-wire output (Donovan & Spina 1992). The total temperature sensitivity of the hot wire can be absorbed into L and M, and corrections for variations in total temperature are then made using the method outlined in Smits *et al.* (1983).

The typical frequency response of a hot wire was approximately 180 kHz. For the normal wire measurements, this frequency response was well above the frequency content of the energy-containing turbulent motions in the flow. However, the crossed-wire measurements have a higher frequency content, and according to the criterion given by Gaviglio, Anguillet & Eléna (1981), the shear stresses were underestimated by approximately 10%. However, great care was exercised during the tuning of a crossed wire to match the wire frequency responses so as to minimize any phase lag in the signals from the two wires since phase difference can affect the inferred turbulence results significantly.

To check for drift in the calibration coefficients, a second calibration was performed after each run in the experiment. Further checks on the accuracy of the hot-wire measurements included comparisons of mean mass-flux profiles with the profiles found from the Pitot survey, and repeatability in the turbulence profiles. That is, a profile was accepted if a second profile measurement agreed within 10%.

The most important error in the crossed-wire measurement was the possible misalignment of the probe with the incoming flow direction. To correct for angular misalignment, a comparison of the mean output voltages during measurement was made with the mean output during calibration. Using the calibration data, a plot of $\Delta E/\Sigma E$ versus ΣE was constructed, where ΔE is the difference between the mean output voltages from the two anemometers and ΣE is the sum (figure 2). As shown by Abell (1974), this plot can be used to determine the angular misalignment of the crossed-wire probe during measurements. In the present work, typical misalignments

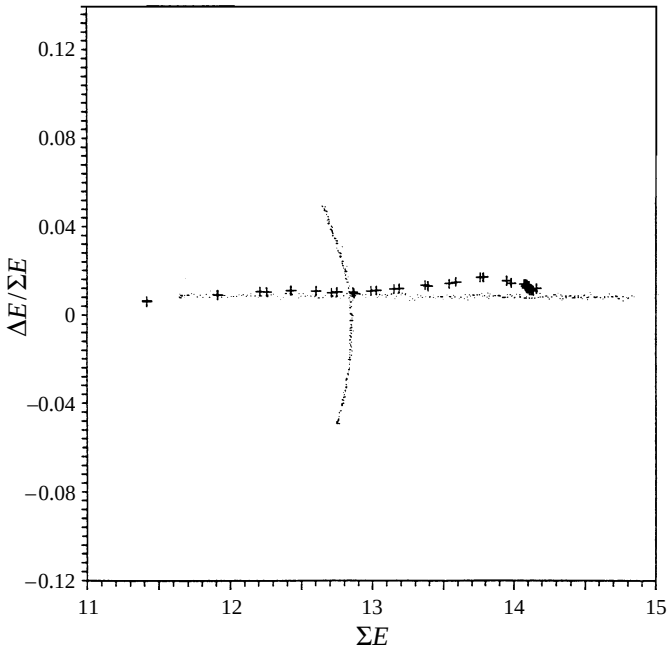

FIGURE 2. Comparison of calibration and experiment mean voltages from a crossed-wire probe revealing the angular misalignment of the probe. The small dots are the calibration data; +, experiment data.

were less than 2° but that is significant enough to require correction. This was achieved by making a simple adjustment to the intercept in the angle calibration.

To deduce a Reynolds stress from the hot-wire output, Morkovin's (1962) 'strong' Reynolds analogy (SRA) was used. This analogy relates the velocity and temperature fluctuations in an equilibrium compressible turbulent boundary layer:

$$\frac{T'}{\overline{T}} = (\gamma - 1)Ma^2 \frac{u'}{\overline{U}}$$

and the correlation coefficient $R_{uT} = -0.8$. The SRA was used to deduce the Reynolds stresses from the output of both the normal and crossed hot wires (for a further discussion of the SRA see Dussauge & Gaviglio 1987; Gaviglio 1987; Spina *et al.* 1991; and Smith & Smits 1993).

The data were acquired using a CAMAC-based system linked to a VAXstation 3100 computer. The mean flow data were filtered through a 10 Hz low-pass filter and acquired at a rate of 200 Hz. The fluctuating data from the hot-wire anemometers were bandpass filtered between 10 Hz and 400 kHz and sampled at 1 MHz. The maximum contiguous data sample for the normal wire and crossed wire measurements was 96K and 48K, respectively. In all surveys at each point in the profile, the stagnation pressure and temperature, and the probe position, were sampled thirty times to find an average value.

To complement the measurements made in this study, three additional sets of measurements obtained by Konrad (1993), Settles *et al.* (1979) and Smits & Muck (1987) were used for the flow upstream of both ramps, the mean flow field and the turbulent flow field on Ramp A, respectively. These measurements were made in the same working section, at the same Mach and Reynolds number as in the

current study. The upstream turbulence measurements by Konrad (1993) were made at the same location as the first of the mean profiles made in the present study ($x = -41$ mm). The measurements by Settles *et al.* (1979) and Smits & Muck (1987) were an essential complement to our measurements as similar measurements would have been extremely difficult with our experimental configuration because of blockage problems. The data from these previous studies should apply unchanged to the present experiments, since the downstream conditions will not affect the upstream conditions so long as the flow is supersonic (note that the subsonic portion of the boundary layer at this Mach number is always small, normally confined to a region below $y/\delta = 0.02$).

3. Results

3.1. *Mean flow measurements*

The wall pressure distribution on Ramp A is shown in figure 3(*a*). At this Mach number and turning angle, the measurements of Settles *et al.* (1979) taken in the same wind tunnel at the same Reynolds number have shown that the flow is separated in the corner with a separation bubble about $0.5\delta_\circ$ in length. Dolling & Murphy (1983) showed that the gradual pressure rise seen in the neighbourhood of the mean separation line is due to the unsteady motion of the separation shock. Immediately downstream of the corner, the pressure increases quickly at first and then more gradually as the flow experiences continued compression and turning on the ramp face. By the end of the ramp, the pressure has reached the inviscid level for 20° of turning at this Mach number. The agreement with previous measurements on the 20° ramp in the same wind tunnel by Settles *et al.* (1979) and Smits & Muck (1987) (not shown) is very good. At the expansion corner, a sharp pressure drop occurs across the corner, after which the pressure continues to decrease for a distance of about $3.5\delta_\circ$ downstream before levelling off. This slow relaxation is due to the interaction of the expansion fan with the Mach number gradient in the boundary layer. The flow downstream of the expansion corner does not reach the level corresponding to an inviscid expansion, but previous studies of expansion-corner flows indicate that the pressure relaxes very slowly, and the extent of our model may have been insufficient to capture the complete relaxation in pressure.

On the concave wall of Ramp B, the pressure begins to rise at the onset of curvature (there is no shock here, and no upstream influence due to unsteady shock motion); it increases along the concave wall, and continues to rise even after the end of curvature (see figure 3*b*). The pressure appears to level off just prior to the beginning of convex curvature, but does not quite reach the pressure level for an isentropic 20° compression at this Mach number. Along the convex wall, the pressure decreases monotonically and continues to decrease for about $2\delta_\circ$ downstream of the end of convex curvature before levelling off. By comparison, the overall pressure changes on Ramp A and Ramp B are similar, but the streamwise pressure gradients are much less severe on Ramp B.

The wall friction distribution along the centreline of Ramp A is shown in figure 4(*a*). The parameter $C_{f,ref}$ is the local wall friction, τ_w, non-dimensionalized by $\frac{1}{2}\rho_{ref}U_{ref}^2$, where ρ_{ref} and U_{ref} are the free-stream density and velocity for the undisturbed flow. Approaching the compression corner, the wall friction rapidly decreases as the flow separates. Downstream of the separation bubble on the ramp face it rises quickly, eventually surpassing the upstream level. Just prior to the expansion corner,

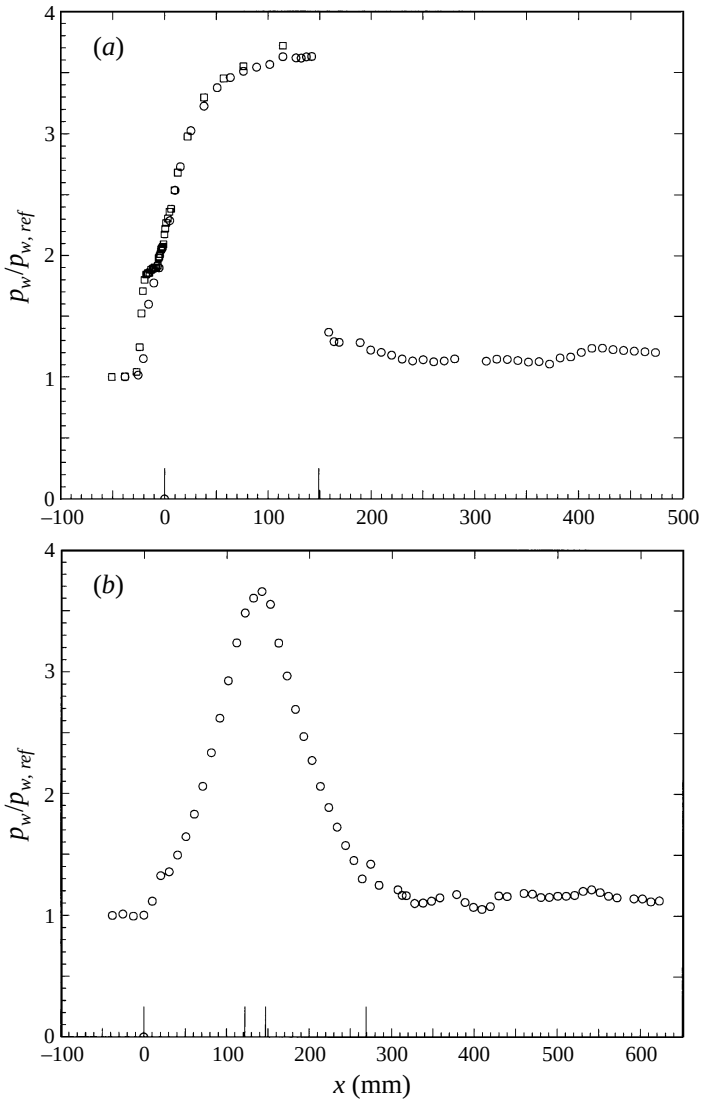

FIGURE 3. Wall pressure distribution: (*a*) along the centreline of Ramp A: ○, Ramp A; □, 20° compression corner (Settles *et al.* 1979); (*b*) along the centreline of Ramp B. The beginning and end of the convave and convex curvatures are marked on the abscissa with vertical lines.

τ_w appears to be levelling off. Downstream of the expansion corner, the wall friction rapidly decreases before approaching an asymptotic value at a distance of about $6\delta_\circ$ downstream of the corner.

In contrast, the wall friction for Ramp B (figure 4*b*) begins to rise at the onset of curvature, increases along the concave wall, and continues to rise after the end of the concave curvature due to the weak adverse pressure gradient that persists in this region. Its highest value occurs in the favourable pressure gradient on the convex wall, $1.8\delta_\circ$ downstream of the peak in the wall pressure. Along the convex wall, the wall friction decreases and continues to decrease after the end of curvature. A consistent difference of about 15% was observed between the wall shear deduced from the Preston tube measurements and the values inferred from the Clauser chart

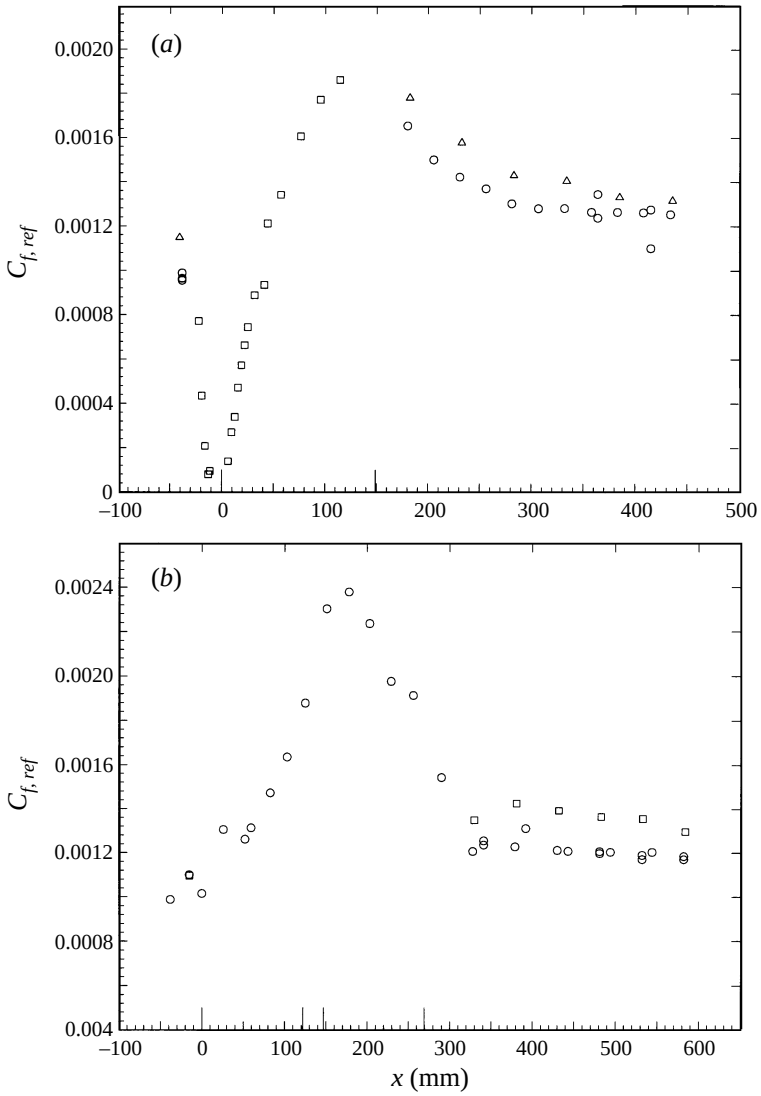

FIGURE 4. Wall friction distribution: (4) along the centreline of Ramp A: ○, Preston tube; □, Preston tube (Settles *et al.* 1979); △, Clauser chart; (*b*) along the centreline of Ramp B: ○, Preston tube; □, Clauser chart. The Preston tube measurements were reduced using the Bradshaw & Unsworth (1974) scheme. For the Clauser chart values, the velocity profiles were transformed using van Driest (1951).

method. Similar discrepancies were noted by Smith *et al.* (1992) in a study of strongly distorted supersonic boundary layers. They suggested that the van Driest (1951) compressibility transformation has errors due to the uncertainty in the boundary layer edge conditions, and therefore the Preston tube measurements are probably more reliable in such cases. As on Ramp A, there was no net reduction in wall friction at the last measurement station. On Ramp B, however, the net increase in the wall friction was about 17%, whereas on Ramp A it was about 28%. Qualitatively, it seems that the change in wall friction depends upon the distance over which the perturbation is applied: the longer the distance, the greater the change.

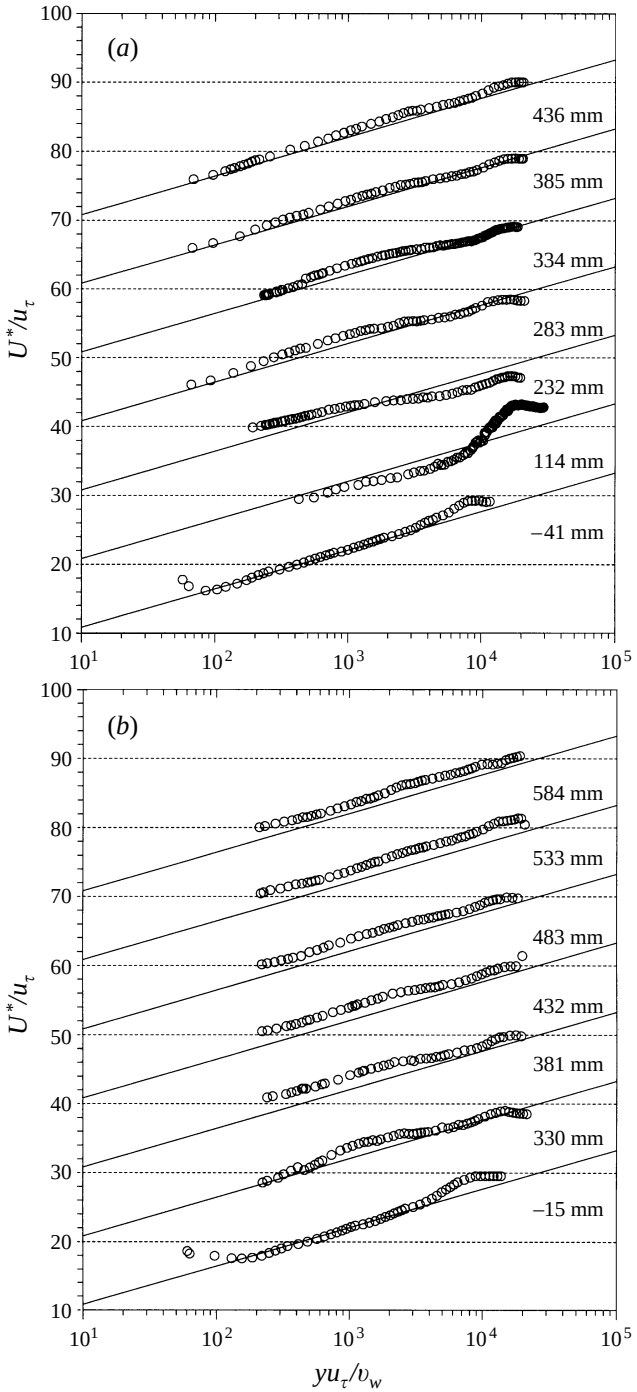

FIGURE 5. The van Driest (1951) transformed velocity profiles on (*a*) Ramp A, (*b*) Ramp B. The profile on the ramp face (114 mm) is from Settles (1975). The values of u_τ used here to scale the profiles were taken from the Preston tube measurements. The profiles have been staggered for clarity.

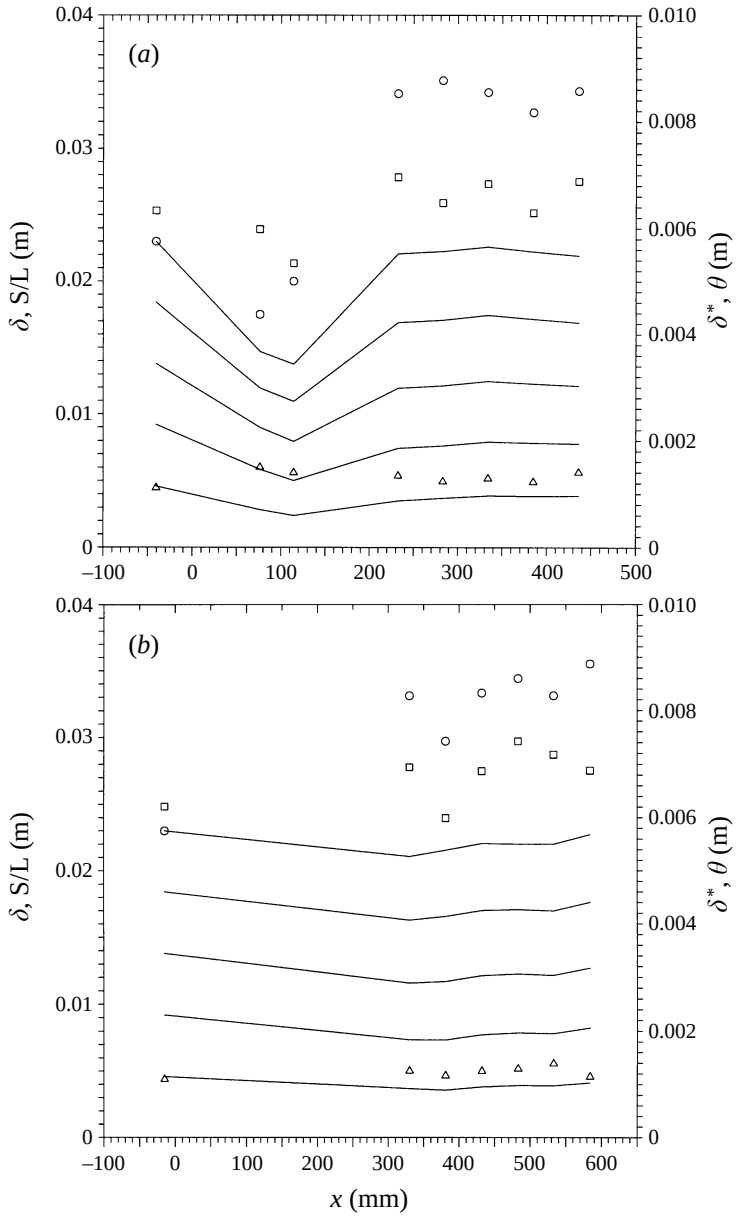

FIGURE 6. The streamwise variation of integral thicknesses and mean streamline heights along (*a*) Ramp A, (*b*) Ramp B: ○, δ; □, δ^*; △, θ; ——, S/L.

The van Driest transformed velocity profiles along the centreline of Ramp A are shown in figure 5(*a*). The upstream profile exhibits a substantial logarithmic region, characteristic of an equilibrium boundary layer. On the ramp face, the wake component increases sharply and a shallow broad dip below the law of the wall appears. Downstream of the expansion corner ($x > 149$ mm), the wake component of the velocity profile collapses while the inner region, initially distorted, quickly recovers. The logarithmic region of the velocity profile is at first absent but reappears at 232 mm and is completely re-established by 283 mm, $5.2\delta_\circ$ downstream of the

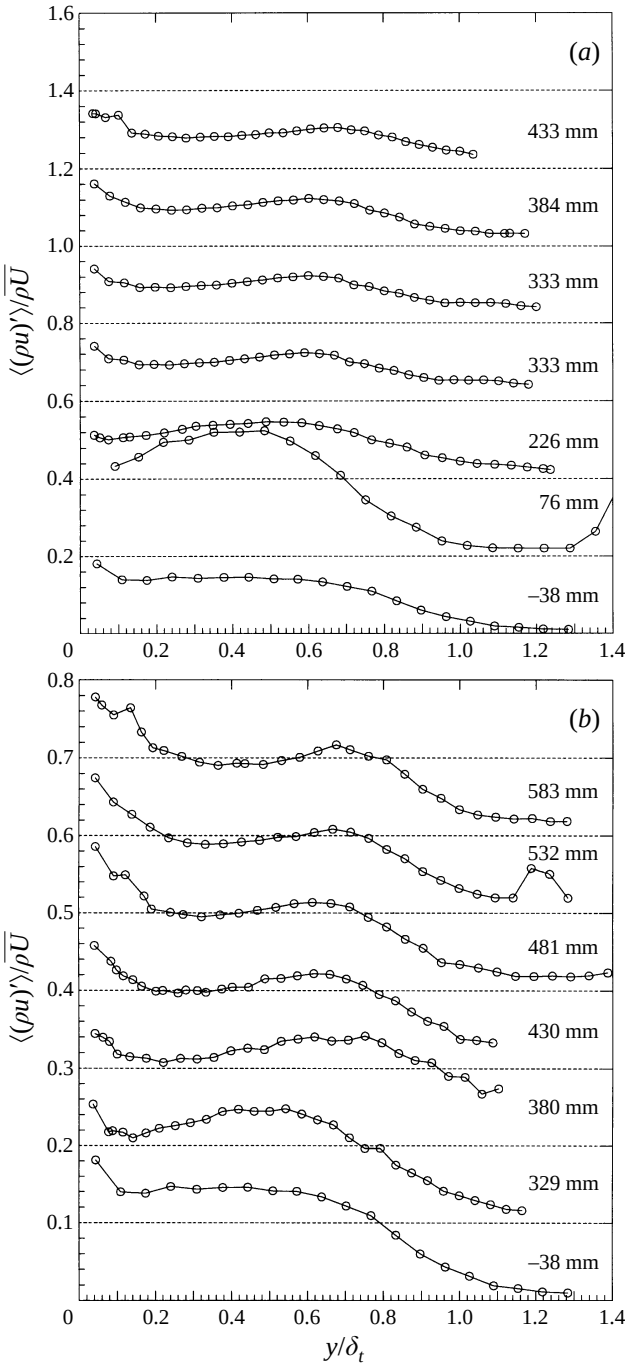

FIGURE 7. Profiles of mass-flux fluctuation intensity, $\langle(\rho u)'\rangle/\overline{\rho U}$, (*a*) on Ramp A (*b*) on Ramp B. The profiles are staggered for clarity.

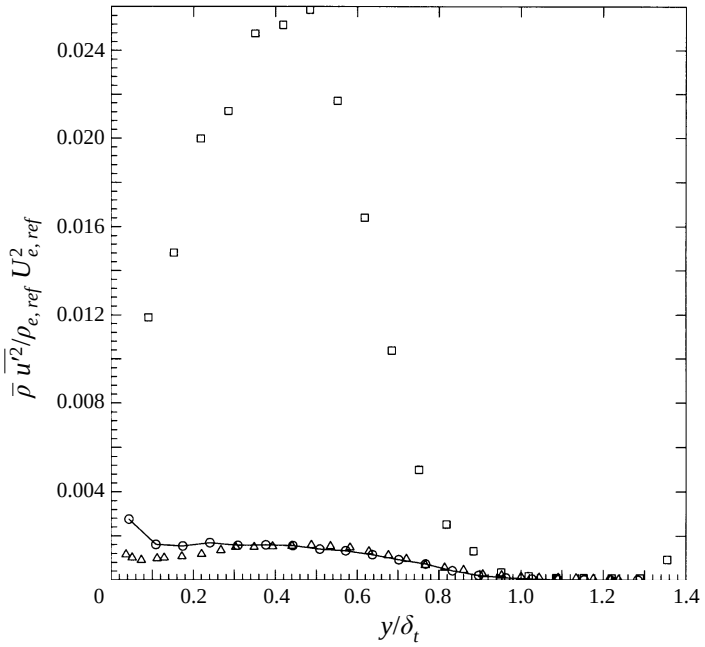

FIGURE 8. Comparison of three streamwise Reynolds stress profiles on Ramp A: ○, −38 mm (upstream of distortions); □, 76 mm (ramp face) (Settles *et al.* 1979); △, 226 mm (downstream of expansion corner).

expansion corner. In contrast, by the last measurement station, $12.5\delta_\circ$ downstream of the corner, the wake is only beginning to recover. The behaviour of the mean velocity profiles closely follows that observed by Zheltovodov *et al.* (1990) in a 25° compression/expansion corner flow at about the same Mach number. By the last measurement station, $28\delta_\circ$ downstream of the expansion corner, Zheltovodov *et al.* found that the wake of the boundary layer still showed very little sign of recovery, and the velocity profile varied logarithmically almost across the entire layer.

The velocity profiles on Ramp B (figure 5*b*) are less dramatic, in that near the wall the profiles all show a substantial region of logarithmic velocity variation suggesting that in the inner region of the boundary layer the rate of application of the distortions was important. However, the recovery of the wake appears to be very similar in the two experiments. At the first measurement station in the relaxation region of Ramp B, $2.6\delta_\circ$ downstream of the end of convex curvature, the wake has collapsed, and the subsequent recovery in the outer layer is slow.

The variation of integral thicknesses and streamline heights on Ramp A are shown in figure 6(*a*). There is some uncertainty in determining the boundary layer thicknesses and the values show considerable scatter. As expected, the boundary layer thickness, δ, on the ramp face is reduced by the compression. The displacement thickness, δ^*, remains relatively unchanged, but the momentum thickness, θ, increases due to continued entrainment. Through the expansion, there is a substantial increase in the boundary layer thickness as a result of the reduced density associated with the expansion. This density change also causes an increase in δ^* in the same region. The variation of the streamline heights downstream of the distortion suggests that the distortion affects the entrainment process. In fact, a mean streamline passing through $y/\delta = 1.0$ at the last measurement station on the ramp is not entrained into the

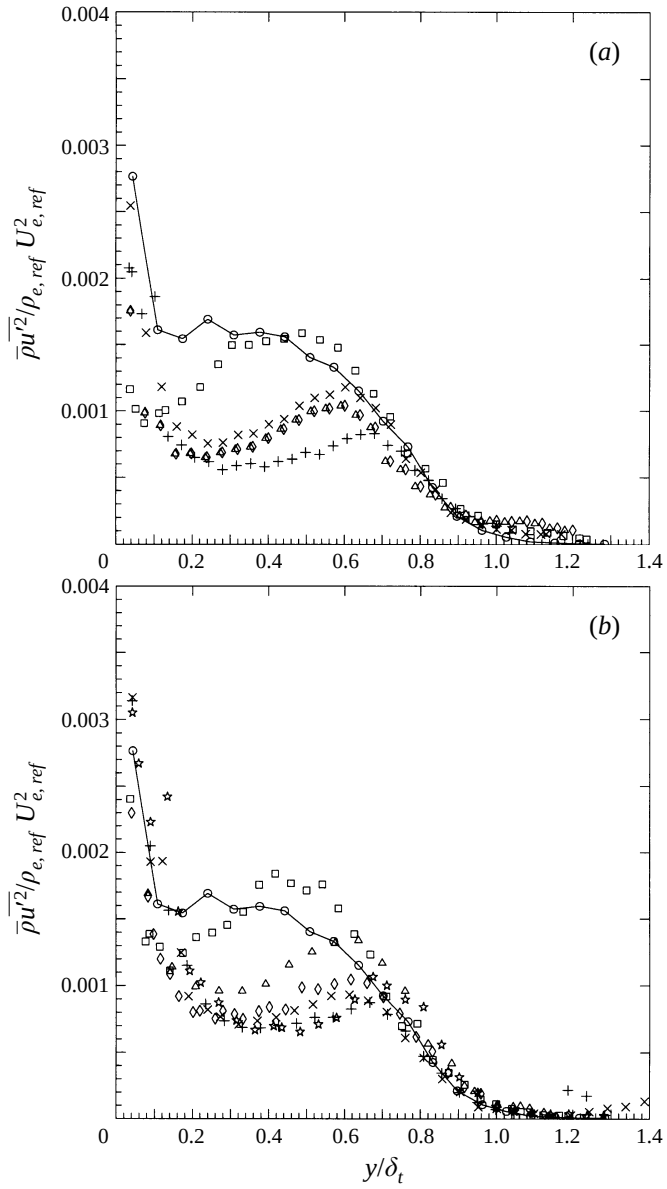

FIGURE 9. Profiles of the streamwise Reynolds stress, $\overline{\rho u'^2}/\rho_{e,ref}\,U^2_{e,ref}$, on (*a*) Ramp A: ○, −38; □, 226.; △, 282; ◇, 333; ×, 384; +, 433. (*b*) Ramp B: ○, −38; □, 329; △, 377; ◇, 430; ×, 481; +, 532; ⋆, 583. Units are in mm.

boundary layer downstream of the expansion; rather, it remains at the edge of the boundary layer.

Similar trends are seen on Ramp B (figure 6*b*). As in Ramp A, the boundary layer thickness grows through the distortion and appears to continue to grow in the relaxation region, probably as a result of continued expansion in the relaxation region. The displacement and momentum thicknesses appear to increase slightly through the distortion, but remain almost fixed in the relaxation region. The variation in the

	x (mm)	z (mm)	δ (mm)	δ_t (mm)	δ^* (mm)	θ (mm)
(*a*)	−41	0	22.8	—	6.1	1.1
	76	−13	17.7	—	6.3	1.6
	114	−13	20.3	—	5.5	1.4
	232	0	34.1	41.3	7.0	1.3
	283	0	35.1	40.0	6.5	1.2
	334	0	34.2	39.3	6.8	1.3
	385	0	32.7	39.4	6.3	1.2
	436	0	34.3	40.2	6.9	1.4
(*B*)	−15	0	22.5	—	6.2	1.1
	330	0	33.1	40.8	6.9	1.2
	381	0	29.7	35.8	6.0	1.2
	432	0	33.3	36.8	6.9	1.2
	483	0	34.4	35.0	7.4	1.3
	533	0	33.1	35.6	7.2	1.4
	584	0	35.5	35.3	6.8	1.1

TABLE 3. Variation in boundary layer thickness and integral thicknesses along (*a*) Ramp A, (*b*) Ramp B

heights of the streamlines exhibit a behaviour similar to that observed in Ramp A, and there is little or no entrainment in the relaxation region.

3.2. *Turbulence measurements*

From figure 7(*a*), it can be seen that the maximum level of the mass-flux fluctuation intensity in Ramp A increases by more than a factor of 2. Downstream of the expansion, however, the maximum intensity level immediately returns almost to its upstream value with a subsequent decrease further downstream. A very similar behaviour is seen on Ramp B (figure 7*b*).

The distortion is much more severe when viewed in terms of the streamwise Reynolds stress, $\overline{\rho}\overline{u'^2}$. Figure 8 emphasizes the severity of the successive distortions presented by Ramp A and their effect on the turbulence in the boundary layer. For example, at a height of $y/\delta = 0.4$, the peak value of $\overline{\rho}\overline{u'^2}$ increases by a factor of 15 through the compression, then returns to the undisturbed level after the expansion. Note that the mean density changes by a factor of 2.4 across each of the distortions, and that the corresponding change in $\overline{u'^2}$ is a factor of 6.3. Clearly, with changes of these magnitudes (see table 2), the turbulence profiles do not scale on local variables such as those proposed by Morkovin (1962).

The streamwise Reynolds stress profiles in the boundary layer downstream of Ramp A are shown in figure 9(*a*). Here, the distance from the wall is scaled on a boundary layer thickness, δ_t, which is the point where the turbulence intensity has reached the free-stream level. The values of δ_t are about 20% larger than the values of δ which were obtained by choosing the point where the total pressure is 99% of the free-stream value (see table 3). In the first profile downstream of the expansion, the intensity level for $y/\delta_t < 0.3$ undershoots the equilibrium value. In contrast, the turbulence in the outer part of the boundary layer displays virtually no cumulative effect of the successive distortions, although with increasing streamwise distance the region of reduced stress occupies an increasingly larger portion of the boundary layer.

As in Ramp A, the effect of the distortions on the streamwise Reynolds stress on Ramp B (figure 9*b*) is first observed near the wall and then 'propagates' into the

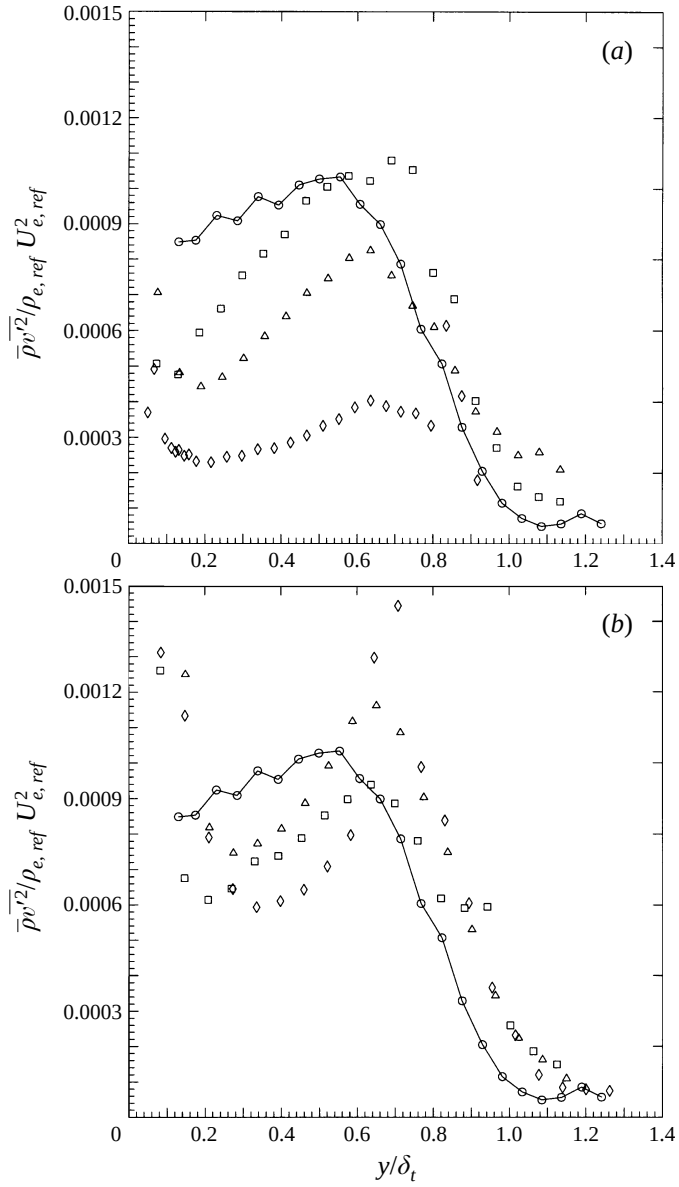

FIGURE 10. Profiles of the normal Reynolds stress, $\overline{\rho v'^2}/\rho_{e,ref}U^2_{e,ref}$, on (*a*) Ramp A: ○, −57 (Konrad 1993); □, 229; △, 330; ◇, 435; (*b*) Ramp B: ○, −57 (Konrad 1993); □, 377; △, 479; ◇, 580. Units are in mm.

layer. For $y/\delta_t > 0.6$, the combined distortions appear to have had little effect on the Reynolds stress. However, in the inner half of the boundary layer, the Reynolds stress rapidly decreases, and at a distance of $7\delta_\circ$ downstream of the end of curvature the stress falls to one-half of the upstream level at $y/\delta_t = 0.3$. This undershoot continues until about $9\delta_\circ$ downstream where the levels appear to have become constant, and the overall stress decrease is not as low as on Ramp A. Further downstream, the Reynolds stress profile is characterized by a steep gradient for $y/\delta_t \leqslant 0.2$, a region of suppressed Reynolds stress for $0.25 \leqslant y/\delta_t \leqslant 0.75$, and a region apparently unaffected

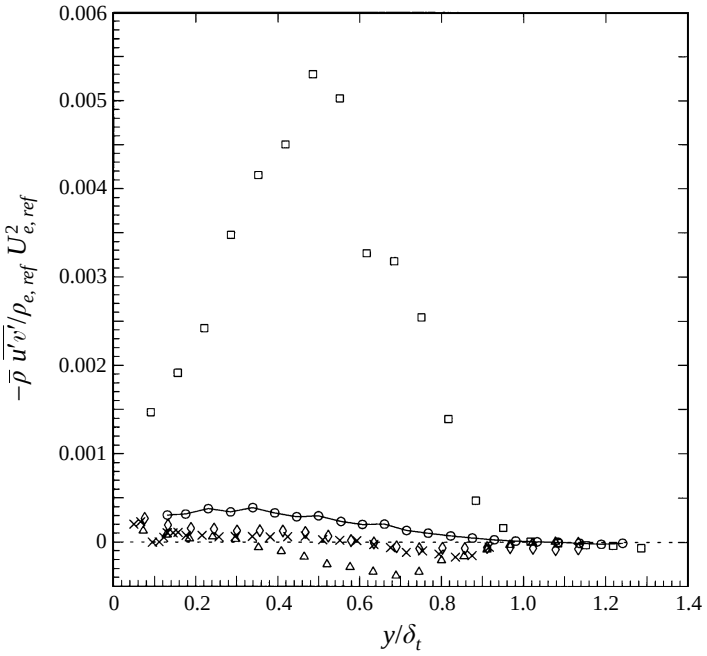

FIGURE 11. A comparison of five Reynolds shear stress profiles, $-\bar{\rho}\overline{u'v'}/\rho_{e,ref}U^2_{e,ref}$ on Ramp A: ○, −57 (Konrad 1993); □, 76 (Smits & Muck 1987); △, 229; ◇, 330; ×, 435.

by the distortions for $y/\delta_t > 0.8$. The change in Reynolds stress mainly reflects changes in the turbulent velocity fluctuations, since the overall change in free-stream mean density is very small (see table 2) and there is only a small change in the shape of the boundary layer density profile.

As noted in §1, Smits *et al.* (1979*b*) described this behaviour as a 'second-order' response, in that the initial overshoot was followed by a tendency for the turbulence intensity to recover to an equilibrium value. In the present case, however, there is little sign of recovery in the region near the wall even at the last measurement station, although the rate of decrease appears to be slowing.

Normal Reynolds stress profiles, $\bar{\rho}\overline{v'^2}$, are shown in figures 10(*a*) and 10(*b*) for Ramps A and B, respectively. The overall behaviour of the normal stress is similar to the streamwise stress, exhibiting a decay in the stress level in the middle of the boundary layer and a region of unaffected stress near the boundary layer edge.

Profiles of the Reynolds shear stress, $-\bar{\rho}\,\overline{u'v'}$, for Ramp A are shown in figures 11 and 12(*a*). At the first measurement station in the relaxation region, the shear stress changes sign, becoming negative in the outer 70% of the boundary layer. This is somewhat unexpected, but the analysis presented in §5 seems to support these observations. At the next two stations, the shear stress has recovered slightly for $y/\delta < 0.5$, but is still only one-third of the upstream level. For $y/\delta > 0.5$, the shear stress has virtually vanished. The Reynolds shear stress behaviour on Ramp B shows a response similar to that seen in Ramp A but to a lesser degree (figure 12*b*). Again, the turbulent shear stress downstream of the end of curvature changes sign between $y/\delta = 0.6$ and the edge of the boundary layer. Further downstream, the shear stress recovers slightly but remains at about one-half of the upstream level, except for $y/\delta > 0.7$ where the shear stress has vanished. Similar observations to those seen here

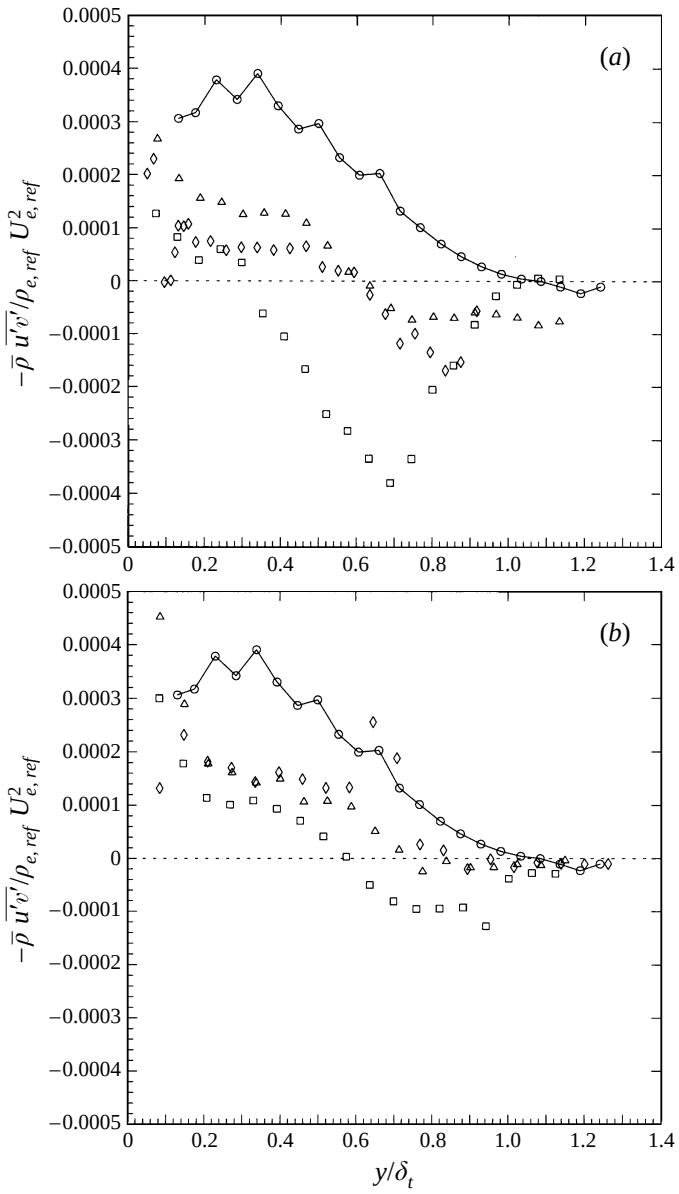

FIGURE 12. Profiles of the Reynolds shear stress on (*a*) Ramp A (*b*) Ramp B. See figure 10 caption for symbol correspondence.

have been made in the outer part of a boundary layer relaxing from convex curvature (So & Mellor 1973; Smits *et al.* 1979*b*) and the response may again be described as 'second-order'.

The anisotropy ratio and the shear correlation coefficient, R_{uv}, are shown in figures 13(a,c) and 13(b,d). In the relaxing boundary layer, these parameters represent the ratios of small quantities and have considerable errors associated with them. Within the accuracy of the measurements, it appears that the anisotropy of the turbulence is relatively unchanged by the successive distortions in both experiments. Note, however, that the anisotropy is quite different from that commonly observed in

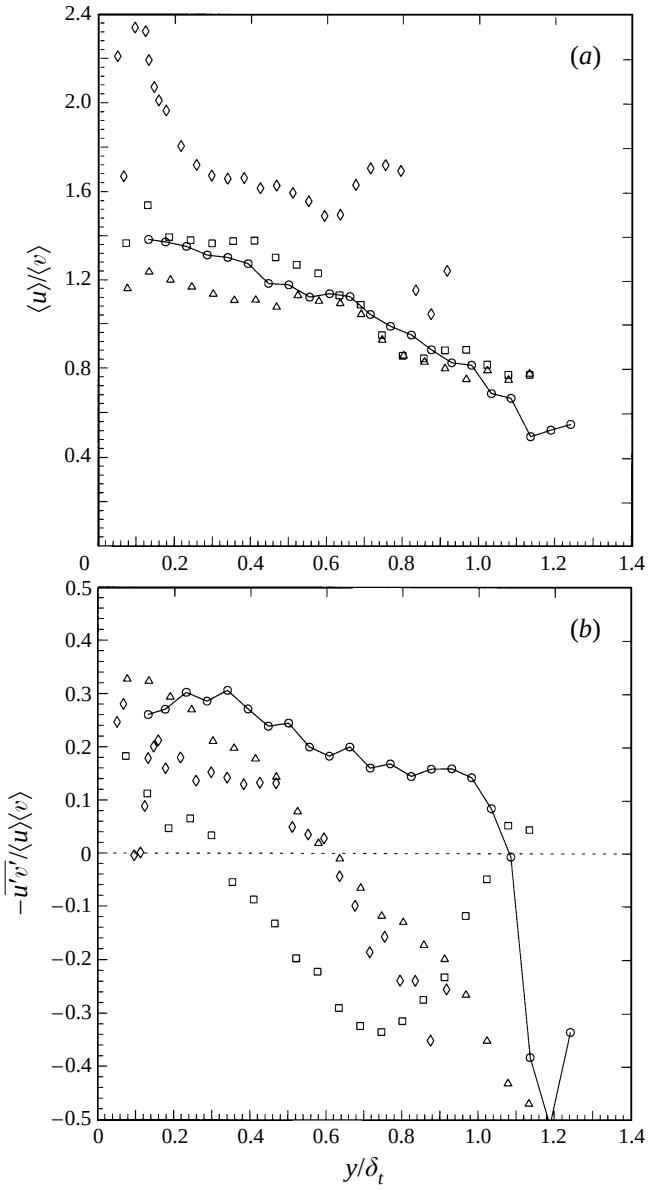

FIGURE 13(*a*, *b*). For caption see facing page.

subsonic boundary layers, and it was suggested by Smits & Dussauge (1996) that the differences are possibly due to Reynolds number effects. Also, the general reduction in the magnitude of R_{uv} reveals a contrast in the response times to the distortion of the diagonal stresses and the shear stress. Apparently, the shear stress reacts very quickly and this is reflected in the first downstream profile. In the subsequent profiles for Ramp A, the shear correlation begins to recover as the normal stresses decay, except in the outer region of the boundary layer where the shear stress has vanished. For Ramp B, R_{uv} recovers rapidly, and at the last measurement station, R_{uv} has almost recovered to the undisturbed levels for the inner 70% of the boundary layer as

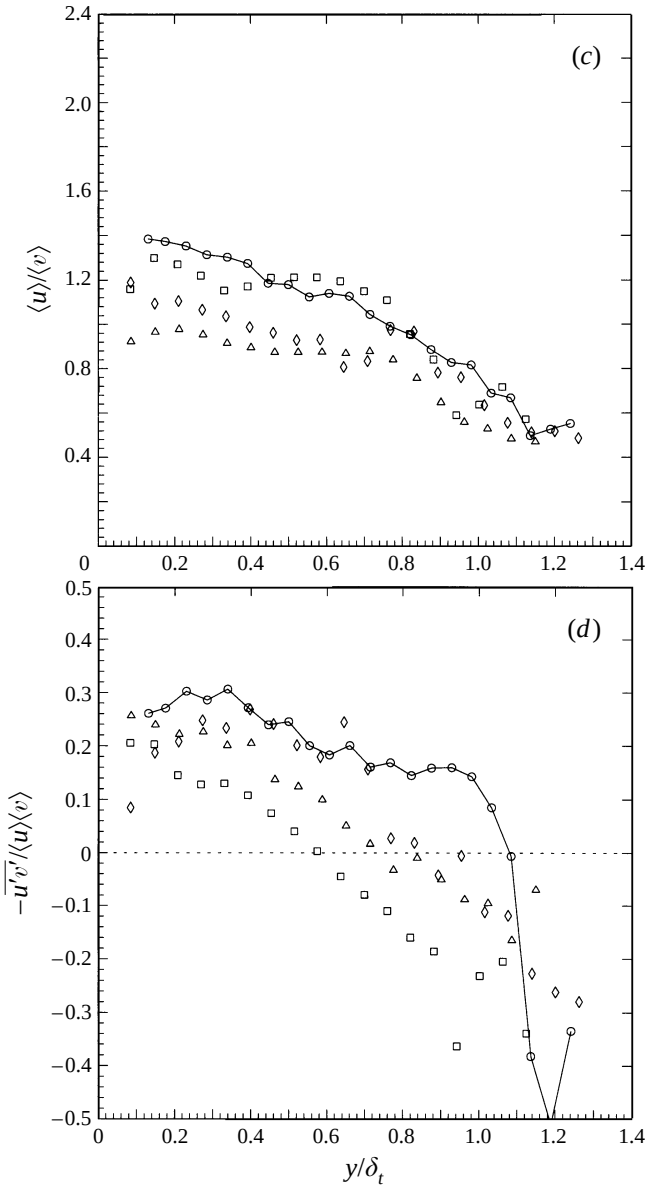

FIGURE 13. Profiles of turbulence structure parameters on (a,b) Ramp A, (c,d) Ramp B.: (a,c) anisotropy ratio, $\langle u'\rangle/\langle v'\rangle$; (b,d) $R_{uv} \equiv -\overline{u'v'}/\langle u\rangle\langle v\rangle$. See figure 10 caption for symbol correspondence.

the turbulence regains, at least partially, its undistorted structure. It is also apparent in these profiles of R_{uv} that the shear stress reacts more quickly to the distortions, particularly in the outer part of the boundary layer. This quick recovery behaviour is similar to that observed by Smits *et al.* (1979*b*) in a subsonic boundary layer relaxing from an impulse in convex curvature. Furthermore, there is no strong indication that a substantial net change in the turbulence structure takes place, and this observation is supported by the earlier works by Jayaram *et al.* (1987) and Fernando & Smits (1990).

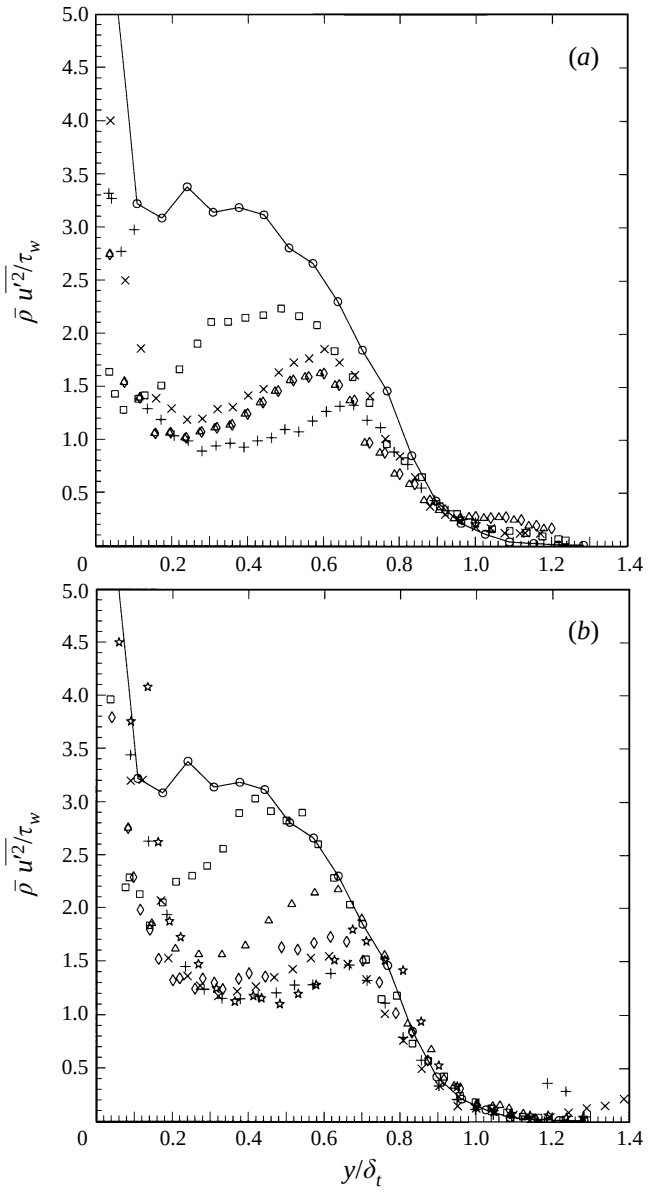

FIGURE 14. Profiles of the streamwise Reynolds stress on Models A and B normalized by local variables, $\bar{\rho}\overline{u'^2}/\tau_w$: (*a*) Ramp A; (*b*) Ramp B. For symbol correspondence see captions for figure 9.

4. Comparison of Ramps A and B

On both ramps, inflection points (local minima and maxima) were found in the streamwise stress profiles for the relaxing boundary layer, and the rate of propagation of the local minimum in the profiles (see figure 9) suggested the existence of an internal layer. As discussed in Smits & Wood (1985), an internal layer represents the region of a perturbed boundary layer which has recovered from the flow distortion, that is, the region where the flow has adjusted to the changed boundary conditions. The mean velocity profiles on both ramps (figure 5) resembled the profiles in a subsonic

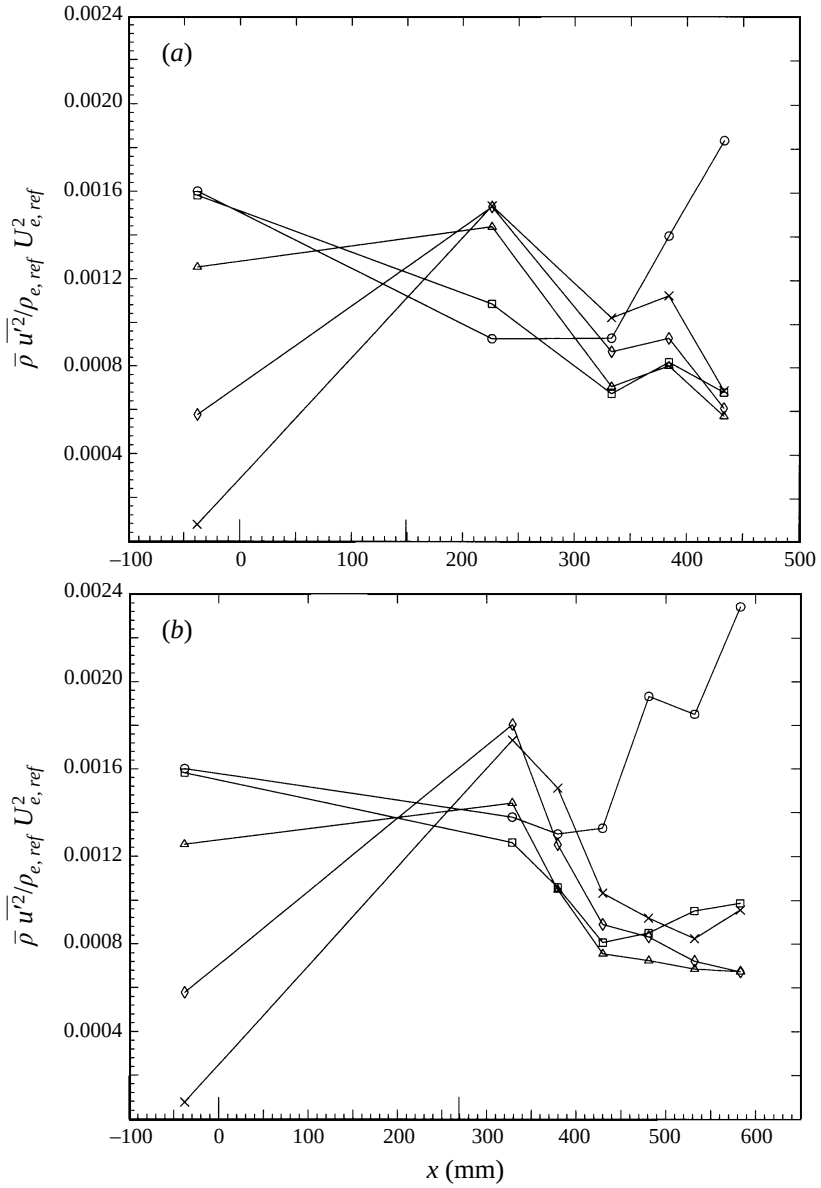

FIGURE 15. The variation of the streamwise Reynolds stress along five streamlines originating in the upstream boundary layer: ○, $0.2\delta_\circ$; □, $0.4\delta_\circ$; △, $0.6\delta_\circ$; ◇, $0.8\delta_\circ$; ×, $1.0\delta_\circ$. (*a*) Ramp A; (*b*) Ramp B.

boundary layer in the early stage of recovery from convex curvature (Baskaran, Smits & Joubert 1987). Figure 14(*a,b*) shows the streamwise velocity fluctuations for both ramps scaled on the local density and wall stress. These profiles display a 'knee-point', as seen by both Baskaran *et al.* (1987) and Alving *et al.* (1990). However, in the small region of the boundary layer where recovery has begun, the profiles could not be collapsed with local scaling arguments. Furthermore, the whole of the boundary layer appears to be far from equilibrium, except perhaps near its edge where effects of the successive distortions seem to cancel.

In general, the overall response of the flow was similar on each ramp. On both

ramps, the streamwise Reynolds stress profiles were characterized by three regions: a region of almost immediate recovery located near the wall (the 'internal' layer), a region in the middle of the boundary layer where the turbulent stress levels were decreasing, and a region near the edge of the boundary layer which was virtually unaffected by the distortions. As part of the relaxation behaviour, all turbulence quantities on both ramps exhibited an undershoot in the central region of the boundary layer.

Despite these overall similarities, distinct differences in the boundary layer responses were observed. For example, the turbulence intensities on Ramp A were generally lower than on Ramp B, and the behaviour of the turbulence depended upon the specific nature of the distortions. This difference was particularly noticeable in the central portion of the boundary layer, where on Ramp B the stress decay was smaller and shorter in duration than on Ramp A (figure 10). In fact, by the end of Ramp B, the decay appeared to have ceased while only appearing to have slowed on Ramp A.

Furthermore, the local extrema appearing in the streamwise Reynolds stress profiles were located at different heights in the boundary layer. On Ramp B where the boundary layer appeared to have a quicker response, both extrema first appeared higher in the boundary layer and remained there further downstream. The turbulence intensities at the points of extrema on Ramp B were also closer to the undisturbed levels than the intensities at the extrema at the same relative positions on Ramp A. Finally, the streamwise stress levels along streamlines originating at five heights in the upstream boundary layer are different (see figure 15). At the furthest downstream locations, the variation on Ramp B showed the beginning of a recovery in all streamlines while at the same relative positions on Ramp A, a recovery was only observed along streamlines originating at $y/\delta_t < 0.4$. Immediately downstream of the expansion, it appears that the boundary layer on Ramp B was beginning to recover while the boundary layer on Ramp A at the same point was still reacting to the distortion. Alternatively, it could be that the expansion on Ramp A reinforced a relaxation process which had already begun on the ramp face, while on Ramp B the expansion distorted a boundary layer which had not fully responded to the distortion due to the initial compression.

Recent measurements by Johnson (1993) suggest that for the geometries he studied (that is, one turning angle and a limited range of $\delta_\circ/R$), the response of a supersonic boundary layer to convex curvature is determined by the total turning angle rather than the radius of curvature. Hence, it may be that the differences observed in the response of the flows over the two ramps are a reflection of the different compression histories. This 'path-dependence' of the turbulence response in compression ramp flows was also noted by Spina *et al.* (1994). Furthermore, in the outer part of the boundary layer, neither series of distortions appeared to have had a dramatic effect on the streamwise intensity levels, and downstream of both distortions, the stress levels in the outer part of the boundary layer were unchanged from the upstream profile. This observation supports the idea that the unsteady shock motion present in Ramp A does not transfer significant mean flow energy to the turbulence: any amplification imparted to the turbulence by the shock wave is reduced by an equal amount in the expansion fan, suggesting a linear response.

5. Relaxation behaviour

To analyse the general relaxation behaviour of the boundary layer downstream of the distortions, we will focus on the flow over Ramp A since the gross features of the

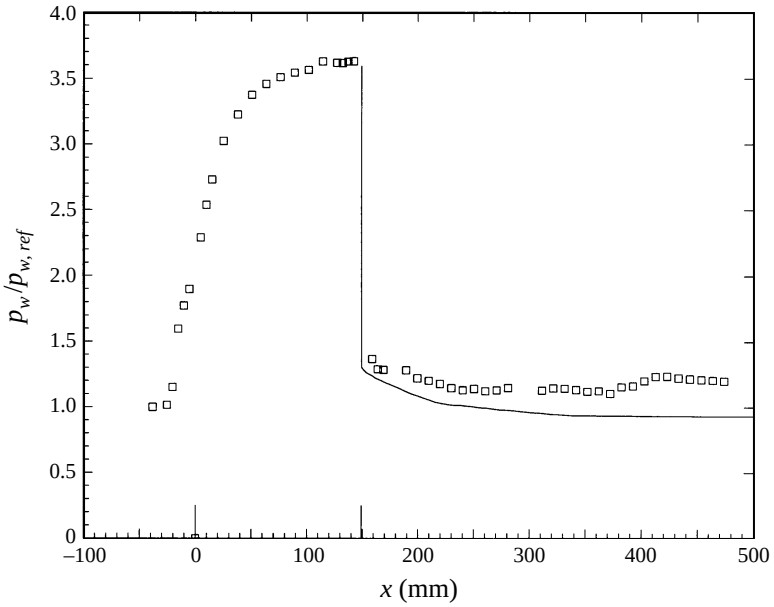

FIGURE 16. A comparison of the computed and experimental wall pressure distribution on Ramp A: □, measured values of wall pressure; —, wall pressure calculated using a rotational method of characteristic algorithm.

boundary layer response were similar in the two flows. As noted earlier, studies of distorted supersonic flows have demonstrated the utility of simplified Reynolds stress calculations for investigating the boundary layer response (Dussauge & Gaviglio 1987; Jayaram *et al.* 1989; Smith & Smits 1991). In these investigations, the evolution of the turbulent flowfield was predicted from the Reynolds stress equations which were simplified and closed using rapid distortion approximations (RDA) (see Dussauge & Gaviglio 1987). Since by design, Ramp A imposed distortions which were more rapid than those imposed by Ramp B, and therefore satisfied the rapid distortion criteria better, we have used RDA methods to help establish qualitative explanations of the observed relaxation behaviour on Ramp A.

The scope of the current study was to use the RDA calculations as a tool towards understanding the important turbulence modifying mechanisms in the distortions. By design, the RDA calculation focuses on the boundary layer response immediately downstream of the distortion ($x < 5\delta_\circ$). Accurate predictions of the Reynolds stress behaviour further into the boundary layer relaxation would require more detailed turbulence modelling. This approach falls outside the scope of an RDA calculation and was not undertaken in the current study. An evaluation of different turbulence models in this type of calculation was made in the earlier study by Jayaram *et al.* (1989), and their evaluations guided the current work. Furthermore, the incoming turbulence for the expansion in Ramp A was not weak and it was far from equilibrium. Consequently, the usual rapid distortion criteria (see Dussauge & Gaviglio 1987) were only weakly satisfied. For example, the ratio of the distortion time scale to the turbulence time scale was 0.63. Hence, the quasi-rapid method developed by Donovan (1989) was employed with the dissipation and return-to-isotropy terms being retained to help account for non-rapid phenomena.

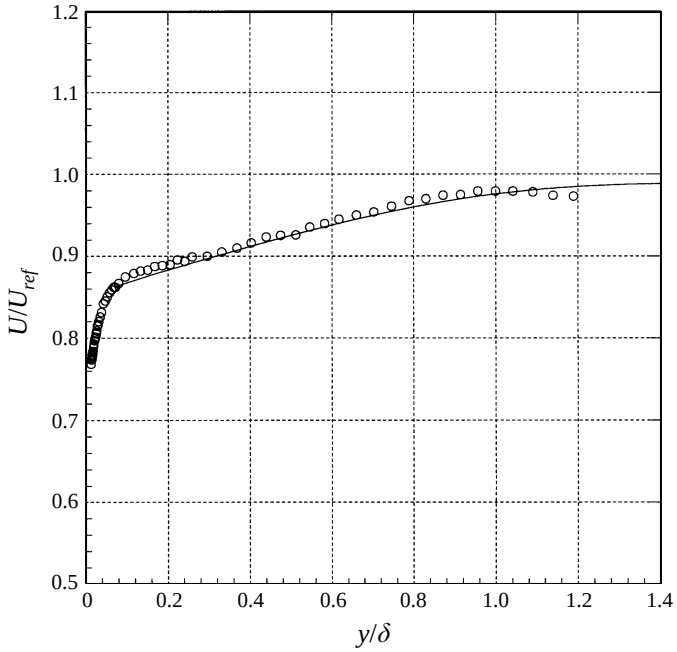

FIGURE 17. A comparison of a computed and an experimental mean velocity profile on Ramp A: ○, experimental profile; —, computed profile. Measurement station is $3.6\delta_\circ$ downstream of the expansion corner.

The rapid distortion assumptions presume a decoupling of the mean and turbulent flow fields. The mean flow can then be treated as inviscid and rotational, and calculated using the method of characteristics (the calculations are confined to the supersonic part of the flow). In figure 16, the calculated wall pressure distribution is compared with the experimental values. The agreement is reasonable, and since it is the flow immediately downstream of the corner that is of immediate interest here, the discrepancies which occur further downstream are not critical. More importantly, the experimental and calculated velocity profiles demonstrate very good agreement (figure 17).

To apply the RDA method, the incoming Reynolds stress tensor must be known. The measurements on the ramp by Smits & Muck (1987) were used as input together with the assumption that $\overline{w'^2}/\overline{u'^2} \approx 0.66$, as found in an equilibrium turbulent boundary layer at a similar Mach and Reynolds number (see Konrad 1993).

The calculated values of the streamwise stress at $x = 229$ mm ($3.6\delta_\circ$) differed from the measured values by a factor of 2 (figure 18). However, if the downstream values are compared with the corresponding values observed on the ramp, it is clear that the rapid distortion method accounts for a large fraction of the observed turbulence attenuation. On the other hand, the calculated shear stress profile at the same location agrees quite well with the measured profile (figure 19), including a region of negative shear stress. This can be understood by considering the Reynolds shear stress transport equation.

For the flow in the expansion, consider the Reynolds stress equations in Favre-averaged variables (Cebeci & Smith 1974) for the shear stress $-\overline{\rho}\widetilde{u'v'}$ and the stream-

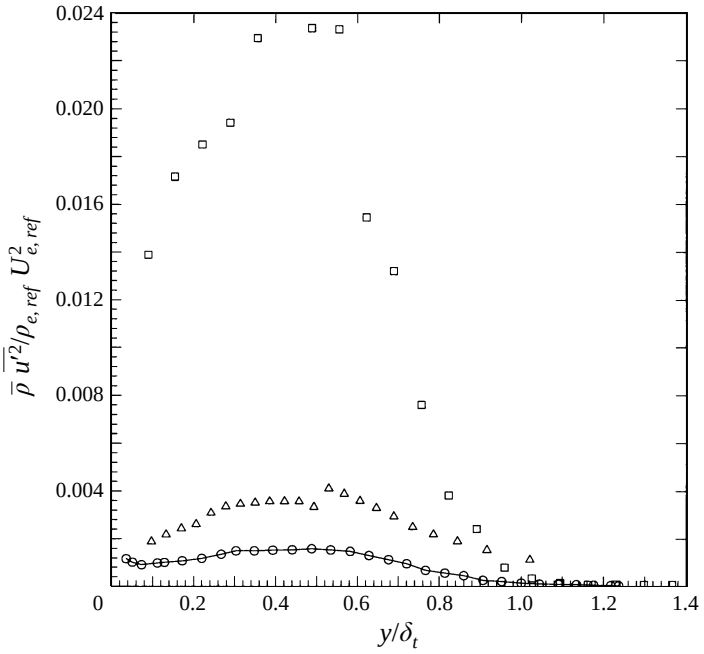

FIGURE 18. A comparison of a computed and experimental streamwise Reynolds stress profile $3.6\delta_\circ$ downstream of the expansion corner on Model A. A stress profile on the ramp face is included for comparison. ○, 229 (experimental); □, 95.2 (experimental); △, 229 (computed). Units in mm.

wise stress $\overline{\rho}\overline{u'^2}$:

$$\frac{\mathrm{D}}{\mathrm{D}t}(-\overline{\rho u'v'}) = \overline{\rho v'^2}\frac{\partial \widetilde{U}}{\partial y} + \overline{\rho u'^2}\frac{\partial \widetilde{V}}{\partial x} + \frac{\partial \overline{\rho u'v'^2}}{\partial y} + \text{Diffusion terms} + \epsilon_D,$$

$$\frac{\mathrm{D}}{\mathrm{D}t}(\overline{\rho u'^2}) = -\overline{\rho u'v'}\frac{\partial \widetilde{U}}{\partial y} - 2\overline{\rho u'^2}\frac{\partial \widetilde{U}}{\partial x} - \frac{\partial \overline{\rho u'^2 v'}}{\partial y} + \text{Diffusion terms} + \epsilon_D.$$

In the evolution of the shear stress, an additional production term becomes important because of the streamline curvature, namely $\overline{\rho u'^2}\partial \widetilde{V}/\partial x$. Near the wall where $\partial \widetilde{U}/\partial y$ is large, this additional term is negligible when compared with the main production term, $\overline{\rho v'^2}\partial \widetilde{U}/\partial y$. However, in the middle of the boundary layer where $\partial \widetilde{U}/\partial y$ decreases, the relative influence of $\partial \widetilde{V}/\partial x$ becomes larger. Furthermore, the streamwise Reynolds stress profile immediately upstream of the expansion corner has a pronounced peak in the middle of the boundary layer. Since the curvature is convex ($\partial \widetilde{V}/\partial x < 0$) and the streamwise stress is strongly amplified, a large negative production term appears in the shear stress transport equation. It is possible that this term may be the driving force for the change of sign in the shear stress in the downstream boundary layer.

Consider also the order of magnitude of the terms appearing in the Reynolds stress transport equations given above. By repeating the calculation, successively neglecting terms in the equations and comparing the results with experiment, the processes that dominate the distortion and relaxation behaviour can be identified. The production terms which are typically neglected in the boundary layer approximations for the two stress equations given earlier, $\overline{\rho u'^2}\partial \widetilde{V}/\partial x$ and $-2\overline{\rho u'^2}\partial \widetilde{U}/\partial x$, proved to be an order

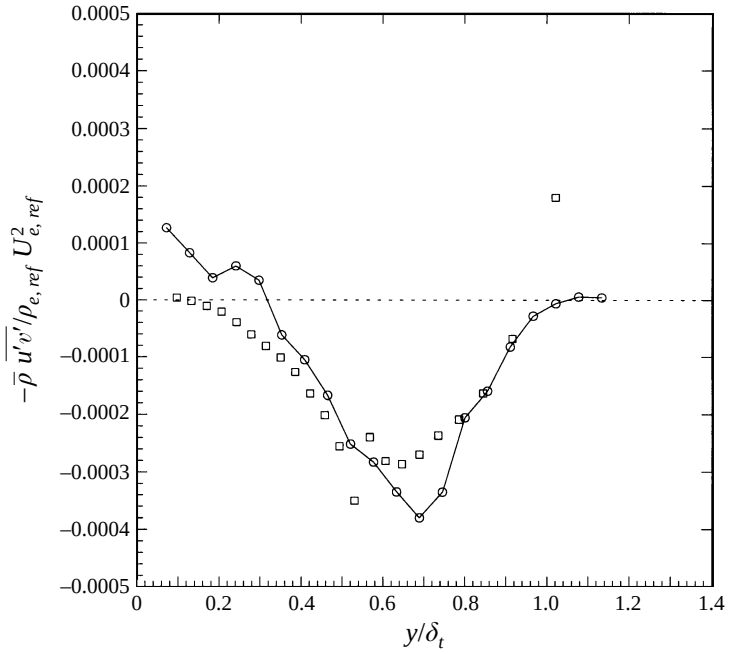

FIGURE 19. A comparison of a computed, □, and experimental, ○, Reynolds shear stress profile $3.6\delta_\circ$ (229 mm) downstream of the expansion corner on Ramp A.

of magnitude larger in the expansion than the production terms typically retained, $\overline{\rho v'^2}\partial\widetilde{U}/\partial y$ and $-\overline{\rho u'v'}\partial\widetilde{U}/\partial y$. In fact, in the outer region of the boundary layer, the production terms along with the effects of dilatation appear to dominate. For the shear stress, these combined effects account for approximately 60% of the decrease in the expansion. For the streamwise stress in the expansion, the additional production term and the main production term (which changes sign due to the strong gradients present in the expansion) become large sinks of turbulence energy. It is not surprising to find that the effect of dilatation is so strong. In a similar expansion-corner flow, Smith & Smits (1991) found that 90% of the change in the streamwise Reynolds stress was due solely to bulk dilatation. In fact, it appears that in strongly expanded flows, dilatation dominates the initial response of the turbulence. Further downstream, however, the striking similarity between the streamwise Reynolds stress measurements presented here and the measurements made by Smits *et al.* (1979*b*) in a subsonic turbulent boundary layer recovering from an impulse of curvature suggests that the long-term relaxation behaviour is largely determined by the long-lasting effects of curvature.

The measurements can also be used to determine the magnitude of the turbulent diffusion terms which appear in the Reynolds stress transport equations. The turbulent diffusion terms $\partial\overline{\rho u'v'^2}/\partial y$ and $-\partial\overline{\rho u'^2v'}/\partial y$ assume large negative values in the middle of the boundary layer at the first station downstream of the expansion. In the shear stress equation, the diffusion term (which in this case acts as a sink of energy in the middle of the boundary layer) combines with the diminished production term to inhibit the recovery of the shear stress. In contrast, for the streamwise stress the diffusion term is a 'source' of energy in the middle of the boundary layer. In this region, the streamwise stress profile decays with streamwise distance (figure 19). It

appears that the large diffusion term transfers energy from the outer region of the boundary layer to recover the deficit closer to the wall.

From this analysis, it appears that the additional production terms and the strong turbulent diffusion processes may be the driving forces behind the dramatic reduction in the shear stress and its subsequent slow recovery. Furthermore by interacting with the turbulent shear, the mean velocity transfers energy from the outer region of the boundary layer, where it resides in the mean flow, to the wall. At the wall, the energy is converted to turbulence energy by the interaction of the turbulent shear stress with the mean velocity gradient. Turbulent diffusion then carries some of this energy back to the outer region of the boundary layer. Since each step of this cycle is dependent upon the Reynolds stresses, the reduction of these stresses at any level in the boundary layer interrupts the transfer of energy. As a result the mean and turbulent flow decay quickly (Townsend 1976).

The combination of compression–expansion distortions appears to be effective in reducing all mechanisms for turbulence energy production. The collapse of the shear stress and the fuller shape of the mean velocity profile inhibit the production of energy in the normal components. In turn, the low levels of normal stresses prevent a recovery of the shear stress. Together these phenomena reinforce the non-equilibrium state of the boundary layer and suggest a very slow recovery.

6. Conclusions

Two flows were considered in which a supersonic turbulent boundary layer was subjected to two successive distortions of equal but opposite sign. The distortions on Ramps A and B were designed such that the flow experienced the same changes in curvature and pressure, but with different histories. Measurements in the boundary layer downstream of the distortions revealed that the different flow histories appeared to have had little effect on the net response of the boundary layer. For example, although the flow response in the two interactions are different in detail, the wall friction distributions relaxed in both ramps to approximately the same levels downstream. Similarly, on both ramps, the wake initially collapsed and recovered very slowly so that at the last measurement station a logarithmic variation in velocity was observed across nearly the entire layer.

The general shape of the streamwise Reynolds stress profiles suggested three zones of response: a recovery region near the wall where the turbulence recovered quickly from the perturbations; a zone of strong response in the middle of the boundary layer where the turbulence undershot the equilibrium distribution sharply in response to the combined effects of the perturbations (second-order response); and a zone of advection near the edge of the boundary layer where the turbulence appeared unaffected by the overall effects of the perturbations (linear response). This latter observation further supported the conclusion of Selig & Smits (1991) that at this Mach number shock-wave oscillation does not contribute to turbulence amplification in shock-wave/boundary layer interactions.

A number of factors combined to inhibit the turbulence production mechanisms in the relaxing boundary layer. These factors included a fuller velocity profile, a decay of the streamwise stress, and a collapse of the shear stress in the expansion fan. As a result, a long recovery period may be expected.

Over most of the boundary layer flow immediately downstream of the distortions, the shear stress appeared to change sign. This observation was supported by an analysis based on rapid distortion approximations. A subsequent recovery of the shear

stress was observed in the lower 60% of the boundary layer, but in the remaining part of the boundary layer, the shear stress was negligible. In the expansion, estimates of the production terms in the Reynolds stress equations revealed that 'negative' production can occur and may be largely responsible for the change of sign in the shear stress observation, and the complex nature of the relaxation process. Not unexpectedly, this indicates that the conventional eddy viscosity approaches to turbulence modelling have severe limitations for these strongly perturbed flows.

This work was supported by AFOSR Grants F49620-93-0064, F49620-93-1-0427, F49620-93-1-0476 and F49620-93-1-0478.

REFERENCES

Abell, C. J. 1974 Scaling laws for pipe flow turbulence. PhD Thesis, University of Melbourne.

Allen, J. M. 1977 Reevaluation of compressible-flow Preston tube calibrations. *NASA TM* X-3488.

Alving, A. E., Smits, A. J. & Watmuff, J. H. 1990 Turbulent boundary layer relaxation from convex curvature. *J. Fluid Mech.* **211**, 529–556.

Ardonceau, P. L. 1984 The structure of turbulence in a supersonic shock-wave/boundary-layer interaction. *AIAA J.* **22**, 1254–1262.

Arnette, S., Samimy M. & Elliott, G. 1993 The effect of expansion on the large-scale structure of a turbulent boundary layer in a supersonic flow. *AIAA Paper* 93-2991.

Bandyopadhyay, P. R. & Ahmed, A. 1993 Turbulent boundary layers subjected to multiple curvatures and pressure gradients. *J. Fluid Mech.* **246**, 503–528.

Baskaran, V., Smits, A. J. & Joubert, P. N. 1987 A turbulent flow over a curved hill. Part 1. Growth of an internal boundary layer. *J. Fluid Mech.* **182**, 47–83.

Bradshaw, P. 1973 Effects of streamline curvature on turbulent flow. *AGARDograph* 169.

Bradshaw, P. & Unsworth, K. 1974 Comment on 'Evaluation of Preston tube calibration equations in supersonic flow.' *AIAA J.* **12**, 1293–1296.

Cebeci, T. & Smith, A. M. O. 1974 *Analysis of Turbulent Boundary Layers*, Academic.

Clauser, F. H. 1956 The turbulent boundary layer. In *Advances in Applied Mechanics*, Vol. IV. Academic.

Debiève, J. F., Gouin, H. & Gaviglio, J. 1982 Evolution of the Reynolds stress tensor in a shock wave-turbulence interaction. *Indian J. Tech.* **20**, 90–97.

Dolling, D. S. & Murphy, M. T. 1983 Unsteadiness of the separation shock wave structure in a supersonic compression ramp flowfield. *AIAA J.* **21**, 1628–1634.

Donovan, J. F. 1989 The structure of supersonic turbulent boundary layers subjected to concave surface curvature. PhD Thesis, Princeton University.

Donovan, J. F. & Spina, E. F. 1992 An improved analysis method for cross-wire signals obtained in supersonic flow. *Exps. Fluids* **12**, 359–368.

Donovan, J. F., Spina, E. F. & Smits, A. J. 1994 The structure of a supersonic turbulent boundary layer subjected to concave surface curvature. *J. Fluid Mech.* **259**, 1–24.

Driest, E. R. van 1951 Turbulent boundary layer in compressible fluids. *J. Aero. Sci.* **18**(3), 145–160.

Dussauge, J.-P. & Gaviglio J. 1987 The rapid expansion of a supersonic turbulent flow: role of bulk dilatation. *J. Fluid Mech.* **174**, 81–112.

Fernando, E. M. & Smits, A. J. 1990 A supersonic turbulent boundary layer in an adverse pressure gradient. *J. Fluid Mech.* **211**, 285–307.

Fernholz, H. H. & Finley, P. J. 1980 A critical commentary on mean flow data for two-dimensional compressible turbulent boundary layers. *AGARDograph* 253.

Gaviglio, J. 1987 Reynolds analogies and experimental study of heat transfer in the supersonic boundary layer. *Intl J. Heat Mass Transfer* **30**, 911–926.

Gaviglio, J., Anguillet, J. P. & Eléna, M. 1981 On the application of hot-wire anemometry to the solution of problems arising in variable temperature turbulent flows. *Recherche Aerospatial* **1**, 59–66.

Gillis, J. C. & Johnston, J. P. 1983 Turbulent boundary-layer flow and structure on a convex wall and its redevelopment on a flat wall. *J. Fluid Mech.* **135**, 123–153.

HOPKINS, E. R. & KEENER, E. R. 1966 Study of surface Pitots for measuring turbulent skin friction at supersonic Mach numbers on adiabatic walls. *NASA TN* D-3478.

JAYARAM, M., DONOVAN, J. F., DUSSAUGE, J.-P. & SMITS, A. J. 1989 Analysis of a rapidly distorted, supersonic turbulent boundary layer. *Phys. Fluids* A **1**, 1855–1864.

JAYARAM, M., TAYLOR, M. W. & SMITS, A. J. 1987 The response of a compressible turbulent boundary layer to short regions of concave surface curvature. *J. Fluid Mech.* **175**, 343–362.

JOHNSON, A. W. 1993 Laminarization and retransition of turbulent boundary layers in supersonic flow. PhD Thesis, Yale University.

KIM, K. S., LEE, Y. & SETTLES, G. S. 1991 Laser interferometer/Preston tube skin-friction comparison in shock/boundary-layer interaction. *AIAA J. Tech. Note* **29**, 1007–1009.

KONRAD, W. 1993 A three-dimensional supersonic turbulent boundary layer generated by an isentropic compression. PhD Thesis, Princeton University.

KOVÁSZNAY, L. S. G. 1950 The hot-wire anemometer in supersonic flow. *J. Aero. Sci.* **17**, 565–572.

LADERMAN, A. J. 1980 Adverse pressure gradient effects on supersonic boundary-layer turbulence. *AIAA J.* **18**, 1186–1195.

MORKOVIN, M. V. 1962 Effects of compressibility on turbulent flows. In *Mécanique de la Turbulence* (ed. A. J. Favre), pp. 367–380.

ROSHKO, A. & THOMKE, G. J. 1966. Observations of turbulent reattachment behind an axisymmetric downstream-facing step in supersonic flow. *AIAA J.* **4**, 975–980.

SCHLICHTING, H. 1979 *Boundary-Layer Theory*, 7th edn. McGraw-Hill.

SELIG, M. S., ANDREOPOULOS, J., MUCK, K. C., DUSSAUGE, J. P. & SMITS, A. J. 1989 Turbulence structure in a shock wave/turbulent boundary-layer interaction. *AIAA J.* **27**, 862–869.

SELIG, M. S. & SMITS, A. J. 1991 Effect of periodic blowing on attached and separated supersonic turbulent boundary layers. *AIAA J.* **29**, 1651–1658.

SETTLES, G. S. 1975 An experimental study of compressible turbulent boundary-layer separation at high Reynolds number. PhD Thesis, Princeton University.

SETTLES, G. S., FITZPATRICK, T. J. & BOGDONOFF, S. M. 1979 Detailed study of attached and separated compression-corner flowfields in high Reynolds number supersonic flow. *AIAA J.* **17**, 579–585.

SMITH, A. M. O. 1955 On the growth of Taylor-Görtler vortices along highly concave walls. *Q. J. Appl. Maths* **13**, 233–262.

SMITH, D. R. 1993 The effects of successive distortions on a turbulent boundary layer in a supersonic flow. PhD Thesis, Princeton University.

SMITH, D. R., FERNANDO, E. M., DONOVAN, J. F. & SMITS, A. J. 1992 Conventional skin friction measurement techniques for strongly perturbed supersonic turbulent boundary layers. *Eur. J. Mech.* B **11**, 719–740.

SMITH, D. R. & SMITS, A. J. 1991 The rapid expansion of a turbulent boundary layer in a supersonic flow. *Theoret. Comp. Fluid Dyn.* **2**, 319–328.

SMITH, D. R. & SMITS, A. J. 1993 The simultaneous measurement of velocity and temperature fluctuations in the boundary layer of a supersonic flow. *Exp. Thermal Fluid Sci.* **7**, 221–229.

SMITS, A. J. & DUSSAUGE, J. P. 1996 *Turbulent Shear Layers in Supersonic Flow*. AIP.

SMITS, A. J., EATON, J. A. & BRADSHAW, P. 1979*a* The response of a turbulent boundary layer to lateral divergence. *J. Fluid Mech.* **94**, 243–268.

SMITS, A. J., HAYAKAWA, K. & MUCK, K. C. 1983 Constant temperature hot-wire anemometer practice in supersonic flows Part 1: The normal wire. *Exps. Fluids* **1**, 83–92.

SMITS, A. J. & MUCK, K. C. 1987 Experimental study of three shock wave/turbulent boundary-layer interactions. *J. Fluid Mech.* **182**, 291–314.

SMITS, A. J. & WOOD, D. H. 1985 The response of turbulent boundary layers to sudden perturbations. *Ann. Rev. Fluid Mech.* **17**, 321–358.

SMITS, A. J., YOUNG, S. T. B. & BRADSHAW, P. 1979*b* The effect of short regions of high surface curvature on turbulent boundary layers. *J. Fluid Mech.* **94**, 209–242.

SPINA, E. F., DONOVAN, J. F. & SMITS, A. J. 1991 On the structure of high-Reynolds-number supersonic turbulent boundary layers. *J. Fluid Mech.* **222**, 293–327.

SPINA, E. F. & SMITS, A. J. 1987 Organized structures in a compressible turbulent boundary layer. *J. Fluid Mech.* **182**, 85–110.

SPINA, E. F., SMITS, A. J. & ROBINSON, S. K. 1994 The physics of supersonic turbulent boundary layers. *Ann. Rev. Fluid Mech.* **26**, 287–320.

So, R. M. C. & Mellor, G. L. 1973 Experiment on convex curvature effects in turbulent boundary layers. *J. Fluid Mech.* **60**, 43–62.

Sturek, W. B. & Danberg, J. E. 1972*a* Supersonic turbulent boundary layer in adverse pressure gradient. Part I: The experiment. *AIAA J.* **10**, 475–480.

Sturek, W. B. & Danberg, J. E. 1972*b* Supersonic turbulent boundary layer in adverse pressure gradient. Part II: Data Analysis. *AIAA J.* **10**, 630–635.

Tani, I. 1962 Production of longitudinal vortices in the boundary layer along a concave wall. *J. Geophys. Res.* **67**, 3075.

Townsend, A. A. 1976 *The Structure of Turbulent Shear Flows*, 2nd Edn. Cambridge University Press.

Walz, A. 1966 *Strömungs- und Temperaturgrenzschichten.* Braun, Karlsruhe. (English translation: *Boundary Layers of Flow and Temperature*, MIT Press, 1969.)

Zheltovodov, A. A., Trofimov, V. M., Shilein, E. H. & Yakovlev V. N. 1990 An experimental documentation of supersonic turbulent flows in the vicinity of sloping forward and back facing steps. *TPM Rep.* 2013. Institute of Theoretical and Applied Mechanics, Siberian Division of the USSR Academy of Sciences, Novosibirsk, USSR.